haematologica
Journal of the Ferrata Storti Foundation

C-C motif chemokine receptor-like 2 promotes the interferon-γ signaling response in myeloid neoplasms with erythroid differentiation and mutated *TP53*

by Nour Sabiha Naji, Sergiu Pasca, Theodora Chatzilygeroudi, Pablo Toledano-Sanz, Joseph Rimando, Yuju An, Yashvi Hemani, Brandy Perkins, Xinghan Zeng, Conover Talbot, Bogdan Paun, Abdulmuez Abdulmalik, Chen Lossos, Tatianna R. Boronina, Ilias Sinanidis, Panagiotis Tsakiroglou, Priyanka Fernandes, Christopher Esteb, Alexander J. Ambinder, Robert N. Cole, Rena Xian, Ivana Gojo, Suman Paul, Mark J. Levis, Amy E. DeZern, Leo Luznik, Styliani Karanika, Linda S. Resar, Richard J. Jones, Frederick Bunz, Lukasz Gondek, Marios Arvanitis and Theodoros Karantanos

Received: March 4, 2025.
Accepted: July 28, 2025.

Citation: Nour Sabiha Naji, Sergiu Pasca, Theodora Chatzilygeroudi, Pablo Toledano-Sanz, Joseph Rimando, Yuju An, Yashvi Hemani, Brandy Perkins, Xinghan Zeng, Conover Talbot, Bogdan Paun, Abdulmuez Abdulmalik, Chen Lossos, Tatianna R. Boronina, Ilias Sinanidis, Panagiotis Tsakiroglou, Priyanka Fernandes, Christopher Esteb, Alexander J. Ambinder, Robert N. Cole, Rena Xian, Ivana Gojo, Suman Paul, Mark J. Levis, Amy E. DeZern, Leo Luznik, Styliani Karanika, Linda S. Resar, Richard J. Jones, Frederick Bunz, Lukasz Gondek, Marios Arvanitis and Theodoros Karantanos. C-C motif chemokine receptor-like 2 promotes the interferon-γ signaling response in myeloid neoplasms with erythroid differentiation and mutated TP53. Haematologica. 2025 Aug 28. doi: 10.3324/haematol.2025.287740 [Epub ahead of print]

C-C motif chemokine receptor-like 2 promotes the interferon-γ signaling response in myeloid neoplasms with erythroid differentiation and mutated *TP53*

Nour Sabiha Naji[1]*, Sergiu Pasca[1]*, Theodora Chatzilygeroudi[1]*, Pablo Toledano-Sanz[2], Joseph Rimando[3], Yuju An[1], Yashvi Hemani[1], Brandy Perkins[1], Xinghan Zeng[1], Conover Talbot Jr[4], Bogdan Paun[1], Abdulmuez Abdulmalik[1], Chen Lossos[5], Tatianna R Boronina[6], Ilias Sinanidis[1], Panagiotis Tsakiroglou[1], Priyanka Fernandes[1], Christopher Esteb[1], Alexander J. Ambinder[1], Robert N. Cole[6], Rena Xian[5], Ivana Gojo[1], Suman Paul[1], Mark J. Levis[1], Amy E. DeZern[1], Leo Luznik[7], Styliani Karanika[8], Linda S. Resar[9], Richard J. Jones[1], Frederick Bunz[10], Lukasz Gondek[1], Marios Arvanitis[2], Theodoros Karantanos[1]

* Equally contributed authors

1. Division of Hematologic Malignancies and Bone Marrow Transplantation, Department of Medical Oncology, The Johns Hopkins University School of Medicine, Baltimore, Maryland, USA
2. Division of Cardiology, Department of Medicine, Johns Hopkins University, Baltimore, MD, USA
3. Department of Hematology and Medical Oncology, Emory University School of Medicine, GA, USA
4. Institute for Basic Biomedical Sciences, Johns Hopkins University, Baltimore, MD, USA
5. Division of Hematopathology, Department of Pathology, The Johns Hopkins University School of Medicine, Baltimore, Maryland, USA
6. Department of Biological Chemistry, Johns Hopkins University, Baltimore, MD, USA
7. Hematology-Oncology Section, Baylor College of Medicine, Houston, TX, USA
8. Division of Infectious Diseases, Department of Medicine, The Johns Hopkins University School of Medicine, Baltimore, Maryland, USA
9. Division of Hematology, Department of Medicine, Johns Hopkins University, Baltimore, MD, USA
10. Department of Radiation Oncology and Molecular Radiation Sciences, Johns Hopkins University School of Medicine, Baltimore, MD, USA

Corresponding author: Theodoros Karantanos, M.D., Ph.D. Assistant Professor of Oncology, Division of Hematologic Malignancies, Department of Medical Oncology, Sidney Kimmel Comprehensive Cancer Center, Johns Hopkins University, Maryland, MD, USA. Email: tkarant1@jhmi.edu

Funding

TK was supported by NCI Grant K08HL168777, the Leukemia Research Foundation New Investigator Research Grant Program and the MacMillan Pathway to Independence Program Award. SP was supported by NCI Grant K08CA270403, the Leukemia Lymphoma Society Translation Research Program award, the American Society of Hematology Scholar award, and the Swim Across America Translational Cancer Research. RC was supported by Cancer Center Support Grant P30CA006973.

Author contributions: N.S.N, S.P. T.C. and T.K conceived and designed the study and wrote the manuscript. N.S.N, T.C., B.P., C.E. performed the flow cytometry analysis. N.S.N, Y.H., Y.A, X.Z., F.B. and T.K. performed the CRISPR-Cas9 deletion experiments. N.S.N, T.C., Y.A., and Y.H. performed the Western blot analysis. N.S.N, Y.H. and X.Z. performed the quantitative real time PCR. N.S.N., S.P., T.C., L.S.R. and L.G. analyzed publicly available bulk RNA sequencing data, J.R., P.T.S., I.G., L.L. and M.A. analyzed publicly available single-cell RNA sequencing data, T.R.B. and R.N.C. performed the phospho-proteomics analysis, C.T. performed the ingenuity pathway analysis, P.T.S and M.A. performed the gene-set-enrichment analysis, N.S.N., B.P. and T.K. processed the primary samples, N.S.N., T.C., I.S., P.T. S.K., and T.K. performed the xenograft studies. N.S.N., B.P., B.C.P. and T.K. processed the primary samples. N.S.N, B.P., C.E. and T.K. performed the clonogenic assays, A.A., Y.A., N.S.N., and B.P. performed ELISA, P.F., A.J.A., M.J.L, A.E.D., R.J.J. identified patients' samples and provided clinical information, C.L. and R.X. provided pathologic assessment for primary samples, N.S.N., T.K., M.J.L., S.K., L.S.R., A.E.D., R.J.J., F.B., S.P. interpreted the data and edited the manuscript.

Conflict of interest

S.P. is a consultant to Merck, and co-founder, consultant and hold equity in TBD Pharma and T-Bird. S.P. owns equity in Gilead and received payment from IQVIA and Curio Science. The companies named above, as well as other companies, have licensed previously described technologies from Johns Hopkins University. Licences to these technologies are or will be associated with equity or royalty payments to the inventors as well as to Johns Hopkins University. The terms of all of these arrangements are being managed by Johns Hopkins University according to its conflict-of-interest policies.

Data and materials availability: All data are available in the main text or the supplementary materials.

Abstract:

Patients with myeloid neoplasms with loss-of-function *TP53* mutations and erythroid differentiation have poor outcomes, and a better understanding of disease biology is required. Upregulation of interferon-γ (IFN-γ) signaling has been associated with acute myeloid leukemia (AML) progression, selection of *TP53* mutated clones and chemotherapy resistance, but its drivers remain unclear. In this study, we found that the surface receptor C-C motif chemokine receptor-like 2 (CCRL2) is overexpressed in AML with erythroid differentiation and *TP53* mutations compared to other AML subtypes and healthy hematopoietic cells. CCRL2 knockout (KO) suppressed erythroleukemia growth *in vitro* and *in vivo*. Further proteomics and transcriptomics analysis revealed IFN-γ signaling response as the top CCRL2-regulated pathway in erythroleukemia. Our mechanistic studies support direct CCRL2-driven IFN-γ signaling upregulation without a clear effect of exogenous IFN-γ, through phosphorylation of STAT1, which is partially mediated by JAK2. CCRL2/IFN-γ signaling is upregulated in erythroid leukemias, and *TP53* mutated AML and appears to be directly induced by *TP53* KO. Finally, CCRL2/IFN-γ signaling is associated with the transformation of pre-leukemic single-hit *TP53* clones to multi-hit *TP53* mutated AML, increased resistance to venetoclax and worse survival in AML. Overall, our findings support that CCRL2 is an essential driver of cell-autonomous IFN-γ signaling response in myeloid neoplasms with erythroid differentiation and *TP53* mutations and highlight CCRL2 as a relevant novel target for these neoplasms.

Introduction

Erythroid differentiation, bi-allelic *TP53* mutations, and loss of heterozygosity at the *TP53* gene are features associated with adverse biology in myeloid neoplasms[1-3]. Genomic characterization of erythroleukemia has revealed an exceptionally high prevalence of complex karyotype and bi-allelic *TP53* mutations[4, 5], suggesting a possible biologic link between loss of p53 function and erythroid differentiation in malignant hematopoiesis. Myeloid neoplasms with these features show poor response to chemotherapy and venetoclax-based therapies, high incidence of disease relapse, and poor survival[1-3, 6, 7].

Recent studies have highlighted a possible implication of inflammatory signaling, including tumor necrosis factor-α (TNF- α) and interferon-γ (IFN-γ) in the induction of erythroid differentiation and evolution of *TP53* mutated acute myeloid leukemia (AML)[8, 9]. Consistently, upregulation of IFN-γ response signaling in AML blasts has been associated with worse survival and resistance to venetoclax[10]. However, the mechanism of inflammatory signaling upregulation in *TP53* mutated myeloid neoplasms remains unclear, with the central hypothesis being that it is mediated by dysregulation of the immune system in the bone marrow microenvironment[8].

C-C motif chemokine receptor-like 2 (CCRL2) is an atypical chemokine receptor involved in inflammatory signaling activation, typically expressed on the surface of activated neutrophils and monocytes [11]. We found that CCRL2 is upregulated in CD34+ cells from patients with myelodysplastic syndrome (MDS) and blasts from patients with AML arising from MDS compared to healthy cells and de novo AML blasts[12]. Further, we have shown that *CCRL2* silencing suppresses MDS/AML cell growth *in vitro* and *in vivo* and sensitizes them to hypomethylating agents [12, 13].

In this study, we show that AML with loss-of-function *TP53* mutations and erythroid differentiation express the highest levels of CCRL2 across AML subtypes, and that CCRL2 deletion by CRISPR-Cas9 suppresses their growth *in vitro* and *in vivo*. We also identified IFN-γ signaling as the top CCRL2-regulated pathway in these neoplasms and demonstrated that *TP53* deletion directly induces CCRL2/IFN-γ signaling upregulation in AML cells.

Methods

Patients and sample processing

Bone marrow samples were collected from bone marrow aspirations of patients with *TP53* mutations (at least 50% VAF) and complex karyotypes. In accordance with the Declaration of Helsinki and under a research protocol approved by the Johns Hopkins Institutional Review Board, informed consent was procured from all donors before specimen collection. Further details are in *Online Supplementary Methods.*

Cell lines and reagents

Human TF-1, K562, SET2, HEL, and MV-411 cell lines were purchased from the American Type Culture Collection. F36P cells were purchased from Leibniz Institute DSMZ. UKE-1 cells were purchased from Coriell Institute. Further information is in *Online Supplementary Methods.*

Flow cytometry analysis

Cells from healthy controls and patients with AEL and AML cell lines were stained with a PE-conjugated anti-human CCRL2 (BioLegend, #358303) and PE/Cy-7-conjugated anti-mouse CD45 (BioLegend #103113), BV510-conjugated anti-human CD45 (BioLegend, #103137). For the assessment of apoptosis, cells were stained with 7AAD (BioLegend, #420403). More details are in *Online Supplementary Methods.*

CCRL2 and TP53 knockout

Lentiviral vectors expressing CCRL2-targeting sgRNA (pLV [CRISPR]-hCas9:T2A: Puro-U6>hCCRL2[gRNA#162], pLV [CRISPR]-hCas9:T2A: Puro-U6>hCCRL2 [gRNA#177]) or empty pLKO.1-puro lentiviral vector (pLV [CRISPR]-hCas9/Puro-U6>Scramble_gRNA1) was transfected into 293T cells using Lipofectamine 2000 (Thermo Fischer Scientific) for lentiviral supernatant production. Methods used for CCRL2 and TP53 lentiviral knockout are detailed in *Online Supplementary Methods.*

Colony formation assay

A colony was defined as a cell aggregate of >50 cells. Methods are described in *Online Supplementary Methods.*

TF-1 and SET2 xenograft mice

Details are described in *Online Supplementary Methods.*

Mass spectrometry phosphoproteomics analysis

ANOVA method was used to calculate the p-values of mean protein ratios for the biological replicates set up using a non-nested (or unpaired) design. Z-score transformation of normalized protein abundances from a quantitative proteomics analysis using isobaric mass tags was applied before performing the hierarchical clustering based on Euclidean distance and complete (furthest neighbors) linkage. The horizontal dendrogram shows the proteins in samples that clustered together. More details are included in *Online Supplementary Methods.*

Pathway Enrichment Analysis

Mass spectrometry experimental data were processed on the Proteome Discoverer platform, as described: abundance values were grouped and mapped to 7,173 unique proteins, then were imported into Partek Genomics Suite 6.6 (Partek Inc. Saint Louis MO) for further analysis and subsequent comparison of CCRL2 knockout. More details are in *Online Supplementary Methods.*

Western Blotting

Protein extraction was performed. Antibodies are reported in *Online Supplementary Methods.*

Co-immunoprecipitation

Cell lysates incubated with beads were then washed extensively and boiled with 30 µl of loading buffer. Methods used are in *Online Supplementary Methods.*

Single-cell RNA sequencing analysis

Publicly available single-cell RNA sequencing data from two studies was analyzed. Methods used are in *Online Supplementary Methods.*

Bulk RNA sequencing

DESeq2 pipeline (PMID 25516281) was used for gene expression normalization. Details are in *Online Supplementary Methods.*

Quantitative real-time PCR (qPCR)

RNA extraction was performed followed by qPCR. Details are in *Online Supplementary Methods.*

Nuclear and cytoplasmic Fractionation

Details are in *Online Supplementary Methods.*

Publicly available databases

Data from TCGA, Beat AML and DepMap databases was analyzed. Details are in *Online Supplementary Methods.*

Statistical Analysis

Statistical analysis was performed by using GraphPad Prism (GraphPad Software, La Jolla, CA). More details are in *Online Supplementary Methods.*

Results

CCRL2 is upregulated in *TP53* mutated MDS/AML and erythroleukemia

CCRL2 expression in AML primary samples and cell lines was analyzed utilizing The Cancer Genome Atlas (TCGA)[14], Beat AML dataset [15] and DepMap Portal[16] datasets. Using TCGA data, we observed that French American British (FAB) M6 and M7 AML expressed higher *CCRL2* levels compared to other AML subtypes (**Fig. 1A**). Based on data from the Beat AML dataset, *TP53* mutated (MT) AMLs have higher *CCRL2* expression compared to wildtype (WT) ones (**Fig. 1B**). Consistently, AML cell lines with erythromegakaryocytic differentiation (EM) have significantly higher CCRL2 expression than AML cell lines without EM differentiation (**Fig. 1C**).

Next, we assessed CCRL2 expression in bone marrow samples of 15 patients with *TP53* MT MDS/AML with complex karyotype and either one *TP53* mutation of VAF at least 50% or two or more *TP53* mutations and 4 acute erythroid leukemia (AEL) patients based on WHO 2022 criteria [17](**Supplementary Fig. 1A**). Among the 15 *TP53* MT MDS/AML patients, 4 patients were identified to have erythroid predominance (EP) (≥50% of nucleated bone marrow cells were erythroid progenitors) but did not meet AEL criteria. Samples from 16 healthy donors were used as controls. Clinical, pathological, and molecular characteristics of healthy donors and patients are presented in Supplementary **Fig. 1A**, **Supplementary Fig. 1B** and **Supplementary Tables 1 and 2**. The sorting strategy is shown in **Supplementary Fig. 2A, B**. CCRL2 expression was significantly higher in blasts and CD34+ cells from AEL patients and *TP53* MT MDS/AML patients than healthy controls (**Fig. 1D, E**) and in CD34+ cells from AEL patients than *TP53* MT MDS/AML patients (**Fig. 1E**). No significant correlation was found between

CCRL2 expression and VAF or the presence of additional somatic mutations (Supplementary **Fig. 1A**). *TP53* MT MDS/AML patients with EP showed a trend toward higher CCRL2 expression in their blasts and CD34+ cells compared to those without EP (**Supplementary Fig. 1C, D**). Finally, CD34+CD71+ cells from AEL patients and *TP53* MT MDS/AML patients with EP express significantly higher CCRL2 levels than healthy donors' erythroid progenitors (**Supplementary Fig. 1E**). Representative samples of healthy donors, *TP53* MT MDS/AML, and AEL are shown in **Fig. 1F**.

To further assess the effect of *TP53* deletion on CCRL2 expression in AML cells with erythroid differentiation, *TP53* was knocked out (KO) in UKE-1, an erythroleukemic cell line with WT *TP53*, by transducing with sgRNAs targeting *TP53* and selecting by treatment with blasticidin or nutlin-3a, two independent *TP53* knockouts (KOs) were developed (KO1 and KO2) (**Supplementary Fig. 3A**). *TP53* KO UKE-1 cells demonstrated higher CCRL2 expression at protein (**Fig. 1G**) and RNA level (**Supplementary Fig. 3B**).

Finally, RNA-sequencing (RNA-seq) data from a published transgenic *TP53*-deleted erythroleukemia mouse model were analyzed to assess the impact of *TP53* deletion in CCRL2 expression. Li *et al.* demonstrated that deletion of *Trp53* (*Trp53*-/-) in $Jak2^{V617F}$ knock-in (*Jak2*-mut) mice leads to the transformation of myeloproliferative neoplasm (MPN) to AML with erythroid features derived from the megakaryocyte-erythroid progenitor (MEP) compartment[18]. Analysis of RNA-seq data (GSE180851) showed a gradual increase in CCRL2 expression in MEPs associated with *Trp53* loss (from $Jak2^{mut}$ to $Jak2^{mut}Trp53$+/- and $Jak2^{mut}Trp53$-/-) compared to WT MEPs **(Fig. 1H**).

CCRL2 deletion suppresses the clonogenicity of erythroleukemia cells *in vitro* and their growth *in vivo*

To assess the functional effects of CCRL2 expression in erythroleukemia cells, CCRL2 was knocked out in multiple AML cell lines with erythroid features and *TP53* mutations (GM-CSF-dependent TF-1, F36P, and GM-CSF-independent K562, SET2 and HEL) by using two sgRNAs (sgCCRL2 1 and sgCCRL2 2) and scrambled sgRNA (sgControl) as control. Suppression of CCRL2 expression was confirmed by flow cytometry (**Supplementary Fig. 3C-G**). CCRL2 KO suppressed the clonogenicity of these erythroleukemic cells (**Fig. 2A-E**) but had no effect on the clonogenicity of MV4-11 cells, which are *TP53* WT cells with monocytic differentiation (**Supplementary Fig. 3H-I**).

To evaluate the effect of CCRL2 KO on erythroleukemic cells *in vivo*, GFP/Luciferase+ TF-1 and SET2 cells transduced with sgControl or sgCCRL2 (sgCCRL2 1) were injected intravenously in NOD.Cg-*Prkdc*^{scid} *Il2rg*^{tm1Wjl}/SzJ (NSG) mice. No significant differences in engraftment rate were observed, but leukemic growth of sgCCRL2 cells in TF-1 xenografts was significantly suppressed (**Fig. 2F-G**), and mice engrafted with CCRL2 KO TF-1 cells had a significantly improved survival rate compared to those engrafted with CCRL2 WT cells (**Fig. 2H**). Similarly, mice engrafted with CCRL2 KO SET2 cells had suppressed leukemic growth (**Fig. 2I-J**); however, no significant difference in mouse survival was observed (**Fig. 2K**). Mice engrafted with CCRL2 WT TF1 and SET2 cells exhibited a significantly lower disease burden in their bone marrows measured by human CD45+% (**Supplementary Fig. 4A, B**). Overall, these findings suggest that loss of CCRL2 inhibits the growth and clonogenicity of leukemic cells with erythroid differentiation both *in vitro* and *in vivo*.

CCRL2 promotes IFN-γ response signaling in erythroleukemia cells

To identify the most prominent effect of CCRL2 KO on erythroleukemia cells at the protein level, unbiased phospho-proteomics analysis was performed in TF-1 cells transduced

with either sgControl or one of two independent sgRNAs (two replicates (KO1 and KO2) of sgCCRL2 1 and one replicate (KO3) of sgCCRL2 2).

Pathway enrichment analysis of the phospho-proteomics data identified IFN signaling as the top pathway suppressed by CCRL2 KO (**Fig. 3A**). This pathway shares various targets with hyperchemokinemia in influenza, the second most prominent pathway (**Fig. 3A**). Liver X Receptor-Retinoid X Receptor (LXR/RXR) was the top pathway upregulated by CCRL2 KO (**Fig. 3A**). The IFN signaling regulator STAT1 (both long and short isoforms) along with the IFN-γ targets IFIT1, IFIT3, and ISG15 were amongst the top CCRL2 regulated proteins, while various LXR/RXR targets were upregulated by CCRL2 KO (**Supplementary Fig. 5A**). A negative interaction between IFN-γ and LXR/RXR pathways has been described[19, 20], providing some rationale for our finding that CCRL2 promotes IFN signaling and suppresses LXR/RXR (**Supplementary Fig. 5B**). Besides these top genes, various IFN-γ/STAT1 targets are significantly downregulated by CCRL2 KO (**Fig. 3B**).

Next, bulk RNA-seq was performed followed by gene set enrichment analysis (GSEA) using a compilation of pathways from MSigDB[21] in CCRL2 WT or KO SET2 cells (**Supplementary Fig. 5C-E**). IFN-γ gene network activation was the top CCRL2-regulated pathway (**Fig. 3C, Supplementary Fig. 5E**). These results further support that IFN-γ response signaling is the top CCRL2-regulated pathway in erythroleukemia.

To validate our findings, the phosphorylation of STAT1, the main IFN-γ signaling regulator[22] in Tyrosine 701 (Y701) and Serine 727 (S727) was measured in CCRL2 WT and KO TF-1, F36P, and SET2 cells showing suppression of Y701 STAT1 phosphorylation and to a lesser extent S727 STAT1 phosphorylation by CCRL2 KO (**Fig. 4A-C**). Of note, S727 STAT1 phosphorylation was not detected in F36P cells, and Y701 phosphorylation was detected in these

cells only in the presence of GM-CSF (**Fig. 4B**). CCRL2 KO suppressed STAT1 nuclear translocation in TF-1 cells (**Supplementary Fig. 6A**). Consistently, quantitative real-time PCR showed that CCRL2 KO suppresses the RNA levels of 3 representative IFN-γ/STAT1 targets, namely *IFIT3*, *IFI30* and *MT2A* (**Fig. 4D**).

Given that exogenous IFN-γ is critical for the IFN-γ signaling response activation [10], the effect of CCRL2 on the sensitivity of AML cells to exogenous IFN-γ was assessed. CCRL2 KO did not affect the upregulation of *IFIT3* expression in TF-1 cells as a response to exogenous IFN-γ (**Supplementary Fig. 6B**). Consistently, while CCRL2 KO suppressed TF-1 cell growth, this was not affected by treatment with exogenous IFN-γ (**Supplementary Figure 6C**). Interestingly, we identified a modest suppression of IFN-γ receptor (IFNGR) levels in the surface of TF-1 cells by CCRL2 KO in the absence of exogenous IFN-γ (**Supplementary Fig. 6D**). Thus, our findings suggest that CCRL2 likely promotes a cell-intrinsic activation of IFN-γ response signaling rather than the sensitivity of leukemic cells to exogenous IFN-γ.

We have previously shown that CCRL2 promotes JAK2/STAT signaling[12]. The regulation of IFN-γ signaling at the molecular level is complex, involving numerous pathways apart from JAK2/STAT[23]. Y701 phosphorylation of STAT1 is mediated mainly by JAK1/2, but S727 phosphorylation is promoted by AKT and p38/MAPK[24-26]. To investigate possible mediators of the CCRL2-induced STAT1 phosphorylation, our doxycycline-inducible CCRL2 TF-1 cells model (iCCRL2 TF-1) [13] was used. Particularly, iCCRL2 TF-1 cells were treated with 0 or 10 ng/ml doxycycline to induce CCRL2 expression, leading to the induction of cell growth (**Supplementary Fig. 7A**). Treatment of iCCRL2 cells with 10 ng/ml doxycycline induced STAT1 Y701 and S727 phosphorylation, while concurrent treatment with the JAK2 inhibitor fedratinib suppressed Y701 but not S727 phosphorylation (**Fig. 4E**). This finding suggests that

CCRL2 promotes Y701 STAT1 phosphorylation at least partially via JAK2 activation. Consistently with our previous findings[12], co-immunoprecipitation showed that CCRL2 KO is associated with decreased JAK2 and STAT1 interaction in TF-1, F36P, and SET2 cells, while doxycycline treatment is associated with increased JAK2/STAT1 interaction in iCCRL2 TF-1 cells (**Fig. 4F**).

Overall, these findings support that IFN-γ response signaling is the top CCRL2-regulated pathway in erythroleukemia cells and that CCRL2 activates likely a cell-intrinsic IFN-γ signaling response without affecting the response of leukemic cells to exogenous IFN-γ by promoting STAT1 phosphorylation partially via JAK2.

IFN-*γ* response signaling is upregulated in AML with erythroid differentiation and *TP53* mutations

It was recently reported, that IFN-γ response signaling is upregulated in monocytic AML and AML with chromosome 7 deletions[10]. Moreover, bulk RNA sequencing revealed that *TP53* MT AML is associated with IFN-γ signaling compared to *TP53* WT AML samples [9]. Similarly, induction of inflammatory pathways has been associated with the selection of *TP53*-mutated clones during the transformation of MPN to multi-hit *TP53*-mutated AML with erythroid features[8]. Here, we found that CCRL2, which is overexpressed in AML with erythroid differentiation and *TP53* mutations, regulates the expression of a subset of IFN-γ targets.

To assess the expression of this IFN-γ targets subset in AML with erythroid features and *TP53* mutations compared to other AML subtypes, an overall score for 18 genes commonly implicated in IFN-γ signaling and identified as CCRL2-associated genes by our analysis

(*CCRL2, STAT1, IFIT1, ICAM1, CD44, IFIT2, PRKCD, IFIT3, IFI35, ISG15, GBP2, IFIH1, MAPK14, GBP4, IFI6, IRF3, IRF7, IFITM3*) was calculated. Based on TCGA data, AML with erythroid and megakaryocytic (EM) differentiation, FAB M6 and M7, respectively, had a higher overall score than other AML subtypes (**Fig. 5A**). Similarly, AML cell lines with erythroid differentiation had higher CCRL2/IFN-γ signaling score compared to other AML cell lines (**Fig. 5B**). To assess the expression of CCRL2/IFN-γ associated genes in *TP53* mutated AML, we used the Beat AML dataset to compare CCRL2/IFN-γ signaling overall score between *TP53* MT and WT AML. *TP53* MT AML had a higher CCRL2/IFN-γ signaling score than *TP53* WT AML (**Fig. 5C**). CCRL2/IFN-γ signaling score was also higher in *TP53* WT AML samples than healthy CD34+ cells (**Fig. 5C**). Among the top CCRL2-regulated genes *IFIT1* was also significantly overexpressed in *TP53* MT AML samples compared to *TP53* WT ones, and a similar trend was observed for *IFIT3* and *ISG15* (**Supplementary Fig. 7B**). Of note, all three genes were upregulated in AML samples compared to healthy bone marrow mononuclear cells (**Supplementary Fig. 7B**).

To assess the expression of these CCRL2/IFN-γ associated genes in primary samples, publicly available single-cell RNA-seq (scRNAseq) datasets were analyzed. First, an analysis of a publicly available scRNAseq dataset of AML blasts and monocytes from five AML patients that was previously published[27] was performed. Two patients in the dataset had megakaryocytic (AML1) and erythroid (AML5) AML; the other three patients (AML2-4) had non-megakaryocytic, non-erythroid AML (**Fig. 5D**). Most of the CCRL2/IFN-γ associated genes were found to be expressed at a relatively higher level in blasts with erythroid differentiation (**Fig. 5E, Supplementary Fig. 7C**), with the top CCRL2/IFN-γ associated genes *IFIT1*, *IFIT3*, and *ISG15* being among the significantly different ones (**Fig. 5E**). Compared with the other four

patients, the AML patient with erythroid differentiation had upregulated expression of *IFIT1*, *ISG15*and *IFIT3* (**Fig. 5E**).

Next, we reanalyzed scRNA-seq data from a study by van Galen *et al.* [28] who performed scRNA-seq in bone marrow aspirates of 16 AML patients including 3 individuals with *TP53* mutations. Blasts were identified by CD34 and c-KIT (CD117) expression (**Supplementary Fig. 8A**). Most of the CCRL2/IFN-γ associated genes were overexpressed in *TP53* MT AML cells compared to *TP53* WT ones (**Supplementary Fig. 8B**), with *IFIT3*, *IFIH1* and *IFITM3* being the ones with the most notable differences (**Fig. 5F**). Of note, the expression of IFN-γ receptors *IFNGR1* and *IFNGR2* was not found to be significantly different between *TP53* WT and MT samples (**Supplementary Figure 8C**). Using the same dataset, the expression of *IFN*-γ gene (*IFNG*) in CD3+ cells (T-cells) (**Supplementary Fig. 8D**) was compared between *TP53* WT and MT AML patients, showing that patients with *TP53* MT AML expressed relatively lower levels of *IFNG* compared to the WT ones without statistically significant difference (**Supplementary Fig. 8D**).

To further assess if induced IFN-γ response signaling in *TP53* mutated AML is associated with increased IFN-γ secretion in the bone marrow microenvironment, CD3+CD45+ and CD3-CD45+ cells were sorted from 4 *TP53* mutated AML patients and 3 healthy bone marrow donors (**Supplementary Table 1, Supplementary Fig. 9A**). Blasts by dim CD45 and low side scatter were also sorted from the *TP53* mutated AML patients (**Supplementary Fig. 9B**). TF-1 *CCRL2* WT and KO and UKE1 *TP53* WT and KO cells were also plated and cultured. Following 72 hours of cell culture (50,000 cells/ml) in the presence of IL-2, the levels of IFN-γ were measured by ELISA, showing that T-cells from *TP53* MT AML cells secreted relatively lower IFN-γ levels compared to healthy donors and no IFN-γ was secreted by blasts or TF-1 and UKE1 cells under

any condition (**Supplementary Fig. 9C**). Overall, these results support that basal secretion of IFN-γ by T cells, without specific antigen stimulation is not particularly increased in *TP53* mutated AML and that *TP53* mutated leukemic cells do not secrete significant amount of IFN-γ.

Since a cell-intrinsic event potentially links *TP53* mutations and deletions with upregulation of CCRL2/IFN-γ signaling, STAT1 phosphorylation and *IFIT3* RNA levels were compared between *TP53* WT and KO UKE1 cells. *TP53* KO led to a prominent increase in both Y701 and S727 phosphorylation of STAT1 (**Fig. 5H**) and upregulation of the IFN-γ target *IFIT3* (**Fig. 5I**) in UKE1 cells. These results are consistent with the observed increase in CCRL2 expression in UKE-1 cells following *TP53* KO (**Fig. 1G**). Of note, *TP53* KO did not induce IFNGR1 expression in UKE1 cells measured by flow cytometry (**Supplementary Figure 8E**) consistent with the scRNAseq data.

Overall, these findings support that CCRL2/IFN-γ associated genes are upregulated in AML cells with erythroid differentiation and *TP53* mutations compared to other AML subtypes. It is possible that a cell-intrinsic mechanism related to *TP53* deletion may contribute to this phenomenon, which does not appear to be heavily dependent on IFN-γ secretion.

CCRL2/IFN-γ signaling upregulation is associated with selection of *TP53* mutated clones and resistance to venetoclax in AML

Given that the role of IFN-γ response signaling in cancer progression remains unclear[29, 30], we then asked what the possible functional implication of CCRL2/IFN-γ signaling response activation in *TP53* mutated AML is.

First, analysis of publicly available CRISPR-Cas9 data (DepMap portal)[16] revealed that the majority of CCRL2/IFN-γ target genes have a negative gene effect in AML cell lines with

erythroid differentiation and *TP53* mutations (HEL, HEL9217, SET2, TF-1, CMK115, MUTZ8, OCIM2, and F36P) (**Fig. 6A**). On the contrary, treatment of primary AML blasts sorted from 3 independent patients with *TP53* MT AML (**Supplementary Table 1**) with exogenous IFN-γ for 72 hours induced apoptosis of leukemic blasts and decreased the percentage of CD34+CD117+ cells (**Fig. 6B, C**). These findings further support that there may be a functional distinction between cell-intrinsic upregulation of IFN-γ signaling and the response of leukemic cells to exogenous IFN-γ.

It was recently reported that inflammatory signaling might contribute to pre-leukemic clonal evolution toward *TP53* multi-hit mutated secondary AML (sAML) with erythroid features[8]. Analysis of scRNA-seq data from this report showed that pre-leukemic single-hit *TP53* heterozygous clones from patients with MPN that transformed to multi-hit *TP53* mutated sAML have higher expression of the top CCRL2/IFN-γ associated genes *IFIT1*, *IFIT3* and *ISG15* compared to *TP53* heterozygous clones from patients who remained in chronic phase (CP-MPN) (**Supplementary Fig. 9D**). Similarly, a significant subset of CCRL2/IFN-γ associated genes were upregulated in pre-leukemic single-hit *TP53* heterozygous clones from MPN patients that transformed to sAML compared to those who remained in CP-MPN (**Fig. 6D**). These results support that CCRL2/IFN-γ signaling may be implicated in the progression of AML with erythroid features via the selection of *TP53* mutated pre-leukemic clones.

Wang *et al.* recently showed that overexpression of IFN-γ targets and particularly *IFITM3* is associated with lower sensitivity to venetoclax [10]. Other studies have highlighted that *TP53* mutations and erythroid differentiation are associated with higher rates of venetoclax resistance[27]. Analysis of data from Beat AML dataset showed that CCRL2/IFN-γ signaling score is positively correlated with venetoclax IC50, supporting that upregulation of this pathway is

associated with increased resistance to venetoclax (**Fig. 7A**). Based on the expression pattern of the CCRL2/IFN-γ associated genes, patients were separated into two clusters; cluster 2 included those with a high expression of *IFIT2*, *IFIT1*, *IFIT3*, *STAT1*, *IFI6*, *IFIH1*, *ISG15*, *IRF7* while cluster 1 included the rest of the patients (**Supplementary Fig. 9E**). Patients in cluster 2 had significantly higher venetoclax IC50 values compared to cluster 1 patients (**Fig. 7A**), suggesting that the most direct CCRL2/IFN-γ associated genes, including *IFIT1*, *IFIT3*, and *ISG15* are potentially more potent mediators of venetoclax resistance.

To further assess the impact of CCRL2 expression on venetoclax sensitivity, CCRL2 WT and KO TF-1 and F36P cells were treated with increasing doses of venetoclax. CCRL2 KO cells were found to have a higher sensitivity to venetoclax compared to WT cells (**Fig. 7B-C**).

Finally, the impact of CCRL2/IFN-γ signaling score on the survival of AML patients was assessed using Beat AML data, demonstrating a negative impact of this score on the overall survival of AML patients (**Fig. 7D**). Multivariable analysis showed that this effect is independent of *TP53* mutation, cytogenetic risk, and patients' age (**Fig. 7D**).

Taken together, our data support that CCRL2 is overexpressed in AML with erythroid differentiation and *TP53* mutations and its deletion suppresses the growth of erythroleukemia cells. CCRL2 promotes IFN-γ signaling response in these AML subtypes, which appears to be associated with a cell-intrinsic effect and is potentially linked to p53 loss-of-function. CCRL2/IFN-γ associated genes are upregulated in erythroid and *TP53*-mutated AML, and this signaling is associated with selection of *TP53*-mutated pre-leukemic clones, resistance to venetoclax and poor overall survival (**Fig. 7E**).

Discussion

Patients with myeloid neoplasms with erythroid differentiation and *TP53* mutations exhibit very short survival due to poor response to therapies, including venetoclax and have a high incidence of relapse[3, 31-36]. Therefore, a better understanding of disease pathogenesis is required. The role of IFN-γ signaling in myeloid neoplasms remains unclear, but it was recently reported that inflammatory pathways may be implicated in the selection of *TP53* mutated pre-leukemic clones driving disease progression[8] and that this signaling is upregulated in *TP53* mutated myeloid diseases[9]. Upregulation of IFN-γ signaling was also associated with AML progression and resistance to venetoclax[10]. However, the mechanisms implicated in the regulation of IFN-γ signaling in myeloid neoplasms remain unclear, and the leading hypothesis is that secreted IFN-γ in the marrow microenvironment is the primary driver of this pathway.

Here, we found that the surface receptor CCRL2 is overexpressed in MDS/AML with erythroid differentiation and *TP53* mutations associated with complex karyotype compared to other AML subtypes and healthy hematopoietic cells, and its deletion suppresses erythroleukemic cells clonogenicity *in vitro* and growth *in vivo*. CCRL2 is normally expressed in activated macrophages, neutrophils, and NK cells and promotes inflammatory signaling [11, 37, 38]. We have previously found that CCRL2 is overexpressed in progenitors from MDS patients and sAML blasts inducing disease progression [12]. Erythroleukemia shares methylation and transcriptomic features with both AML and MDS [32], suggesting a possible overlap of erythroleukemia biology with MDS and sAML, consistent with our findings. Recent data highlight that the clinical outcomes of MDS/AML spectrum are primarily affected by specific biological characteristics, with loss of p53 function having the most prominent effects and not by the exact blasts' percentage[39]. Based on our published data [12]and our current results, CCRL2

overexpression is probably associated with adverse disease biology within this spectrum, supporting a correlation with loss of p53 function.

Phospho-proteomics and transcriptomics analysis highlighted IFN-γ response signaling as the top CCRL2-regulated pathway in erythroleukemia cells. Activation of inflammatory pathways is consistent with the well-described role of CCRL2 in promoting inflammatory response [11, 37, 38]. Our studies confirmed suppressed nuclear translocation of STAT1 and decreased STAT1 target expression by CCRL2 KO in erythroleukemia cells. Mechanistically, JAK2 is a critical upstream regulator of STAT1 phosphorylation and IFN-γ signaling [40], and we have reported that CCRL2 induces JAK2/STAT signaling[12]. Here, by utilizing our doxycycline-inducible CCRL2 TF-1 cells, we found that CCRL2 induces STAT1 Y701 phosphorylation at least partially via JAK2. While Y701 phosphorylation of STAT1 is mainly mediated by JAK2, other pathways, including p38/MAPK and AKT, potentially induce S727 phosphorylation[24, 25]. Further studies are required to investigate a possible implication of CCRL2 in regulating these pathways to promote STAT1 S727 phosphorylation. Of note, we found that CCRL2 induces IFN-γ response signaling in erythroleukemic cells but does not affect their response to exogenous IFN-γ, suggesting that CCRL2 may regulate this pathway downstream of IFN-γ receptor.

Our CCRL2/IFN-γ associated genes were upregulated in AML with erythroid differentiation and *TP53* mutations based on TCGA, DepMap portal, and Beat AML data. By analyzing scRNAseq data from publicly available datasets, we demonstrated increased expression of CCRL2/IFN-γ associated genes in blasts from erythroid leukemia and *TP53* MT AML compared to other AML subtypes. Importantly, we did not observe a significant difference in *IFNG* expression in T-cells from *TP53* MT AML samples compared to *TP53* WT samples and sorted IL-2 stimulated T-cells from *TP53* MT AML patients secreted relatively lower levels of

IFN-γ compared to healthy donors. This result is consistent with previous studies reporting lower secretion of IFN-γ by T-cells[41] and relatively lower IFN-γ/IFN-γ receptor interactions in *TP53* MT AML samples compared to other AML subtypes such as monocytic AML[10]. These results further support the possible implication of a cell-intrinsic mechanism of IFN-γ response signaling upregulation in *TP53* MT myeloid neoplasms. Indeed, we found that *TP53* KO causes a direct increase in CCRL2 levels, STAT1 phosphorylation, and *IFIT3* expression, suggesting that loss of p53 can directly promote CCRL2/IFN-γ signaling. Given the exceptionally high frequency of *TP53* loss-of-function mutations in erythroleukemia and our finding that *TP53* KO induces CCRL2/IFN-γ signaling, it is possible that upregulation of this pathway is predominantly associated with *TP53* loss-of-function mutations, with particularly high levels of induction of this signaling in *TP53* mutated erythroleukemias.

The functional implication of IFN-γ signaling in cancer progression remains unclear[29, 30]. We showed that deletion of CCRL2/IFN-γ associated genes has a relatively negative impact on erythroleukemia/*TP53* MT AML cells survival. Interestingly, as previously reported[10], *IFITM3* appears to have by far the highest negative gene effect, which could be related to the inconsistency of the effect of CCRL2 on the expression of this gene, which we observed. Consistently, *IFNGR1* silencing or inhibition with neutralizing antibodies induced AML differentiation and suppressed leukemogenesis *in vitro* and *in vivo* [42]. However, exogenous IFN-γ decreases the survival of *TP53* MT AML blasts, suggesting a potentially different effect of exogenous and cell-intrinsic IFN-γ signaling activation. CCRL2/IFN-γ associated gene upregulation was also associated with the transformation of *TP53* MT pre-leukemic clones to multi-hit *TP53* MT AML, increased resistance to venetoclax and worse overall survival consistent with previous findings[8, 10].

Our study has several limitations. While we have performed several experiments investigating the effect of CCRL2 on the activation of IFN-γ signaling as a response to exogenous IFN-γ and the possible implication of secreted IFN-γ, additional mechanistic studies and experiments with antigen-stimulated T-cells are required to solidify these associations. Importantly, while we did not observe a prominent alteration of IFN-γ receptor expression in our *TP53* knockout system and publicly available single-cell RNA sequencing data, additional experiments using IFNGR1 gene editing or IFNGR1 neutralizing antibody will be required to clarify its implication. Finally, future studies including STAT1 gene editing and patient-derived xenografts are needed to investigate further the functional implication of IFN-γ signaling activation on *TP53* mutated AML progression and treatment resistance.

In conclusion, our results support that CCRL2 is overexpressed in AML with erythroid differentiation and *TP53* mutations inducing IFN-γ signaling response in these neoplasms. Based on our studies, a cell-intrinsic phenomenon related to p53 loss of function may contribute to this phenomenon. Activation of this pathway is associated with the selection of *TP53* MT pre-leukemic clones and resistance to venetoclax, supporting further investigation of CCRL2/IFN-γ signaling as a potential therapeutic target for AML with erythroid differentiation and *TP53* mutations.

REFERENCES

1. Alaggio R, Amador C, Anagnostopoulos I, et al. The 5th edition of the World Health Organization Classification of Haematolymphoid Tumours: Lymphoid Neoplasms. Leukemia. 2022;36(7):1720-1748.
2. Almeida AM, Prebet T, Itzykson R, et al. Clinical Outcomes of 217 Patients with Acute Erythroleukemia According to Treatment Type and Line: A Retrospective Multinational Study. Int J Mol Sci. 2017;18(4):837.
3. Daver NG, Maiti A, Kadia TM, et al. TP53-Mutated Myelodysplastic Syndrome and Acute Myeloid Leukemia: Biology, Current Therapy, and Future Directions. Cancer Discov. 2022;12(11):2516-2529.
4. Fang H, Wang SA, Khoury JD, et al. Pure erythroid leukemia is characterized by biallelic TP53 inactivation and abnormal p53 expression patterns in de novo and secondary cases. Haematologica. 2022;107(9):2232-2237.
5. Reichard KK, Tefferi A, Abdelmagid M, et al. Pure (acute) erythroid leukemia: morphology, immunophenotype, cytogenetics, mutations, treatment details, and survival data among 41 Mayo Clinic cases. Blood Cancer J. 2022;12(11):147.
6. Wong TN, Ramsingh G, Young AL, et al. Role of TP53 mutations in the origin and evolution of therapy-related acute myeloid leukaemia. Nature. 2015;518(7540):552-555.
7. Sinanidis I, Hochman MJ, Tsai HL, et al. Favorable outcomes in MDS and oligoblastic AML-MR after reduced-intensity conditioning allogeneic bone marrow transplantation with post-transplantation cyclophosphamide. Bone Marrow Transplant. 2024;59(8):1178-1180.
8. Rodriguez-Meira A, Norfo R, Wen S, et al. Single-cell multi-omics identifies chronic inflammation as a driver of TP53-mutant leukemic evolution. Nat Genet. 2023;55(9):1531-1541.
9. Vadakekolathu J, Lai C, Reeder S, et al. TP53 abnormalities correlate with immune infiltration and associate with response to flotetuzumab immunotherapy in AML. Blood Adv. 2020;4(20):5011-5024.
10. Wang B, Reville PK, Yassouf MY, et al. Comprehensive characterization of IFNγ signaling in acute myeloid leukemia reveals prognostic and therapeutic strategies. Nat Commun. 2024;15(1):1821.
11. Schioppa T, Sozio F, Barbazza I, et al. Molecular Basis for CCRL2 Regulation of Leukocyte Migration. Front Cell Dev Biol. 2020;8:615031.
12. Karantanos T, Teodorescu P, Perkins B, et al. The role of the atypical chemokine receptor CCRL2 in myelodysplastic syndrome and secondary acute myeloid leukemia. Sci Adv. 2022;8(7):eabl8952.
13. Karantanos T, Teodorescu P, Arvanitis M, et al. CCRL2 affects the sensitivity of myelodysplastic syndrome and secondary acute myeloid leukemia cells to azacitidine. Haematologica. 2023;108(7):1886-1899.
14. Bagger FO, Sasivarevic D, Sohi SH, et al. BloodSpot: a database of gene expression profiles and transcriptional programs for healthy and malignant haematopoiesis. Nucleic Acids Res. 2016;44(D1):D917-924.

15. Tyner JW, Tognon CE, Bottomly D, et al. Functional genomic landscape of acute myeloid leukaemia. Nature. 2018;562(7728):526-531.
16. Boehm JS, Garnett MJ, Adams DJ, et al. Cancer research needs a better map. Nature. 2021;589(7843):514-516.
17. Khoury JD, Solary E, Abla O, et al. The 5th edition of the World Health Organization Classification of Haematolymphoid Tumours: Myeloid and Histiocytic/Dendritic Neoplasms. Leukemia. 2022;36(7):1703-1719.
18. Li B, An W, Wang H, et al. BMP2/SMAD pathway activation in JAK2/p53-mutant megakaryocyte/erythroid progenitors promotes leukemic transformation. Blood. 2022;139(25):3630-3646.
19. Ma F, Liu SY, Razani B, et al. Retinoid X receptor α attenuates host antiviral response by suppressing type I interferon. Nat Commun. 2014;5:5494.
20. Zelcer N, Tontonoz P. Liver X receptors as integrators of metabolic and inflammatory signaling. J Clin Invest. 2006;116(3):607-614.
21. Subramanian A, Tamayo P, Mootha VK, et al. Gene set enrichment analysis: a knowledge-based approach for interpreting genome-wide expression profiles. Proc Natl Acad Sci U S A. 2005;102(43):15545-15550.
22. Mao X, Ren Z, Parker GN, et al. Structural bases of unphosphorylated STAT1 association and receptor binding. Mol Cell. 2005;17(6):761-771.
23. Ivashkiv LB, Donlin LT. Regulation of type I interferon responses. Nat Rev Immunol. 2014;14(1):36-49.
24. Nguyen H, Ramana CV, Bayes J, Stark GR. Roles of phosphatidylinositol 3-kinase in interferon-gamma-dependent phosphorylation of STAT1 on serine 727 and activation of gene expression. J Biol Chem. 2001;276(36):33361-33368.
25. Kovarik P, Stoiber D, Eyers PA, et al. Stress-induced phosphorylation of STAT1 at Ser727 requires p38 mitogen-activated protein kinase whereas IFN-gamma uses a different signaling pathway. Proc Natl Acad Sci U S A. 1999;96(24):13956-13961.
26. Quelle FW, Thierfelder W, Witthuhn BA, Tang B, Cohen S, Ihle JN. Phosphorylation and activation of the DNA binding activity of purified Stat1 by the Janus protein-tyrosine kinases and the epidermal growth factor receptor. J Biol Chem. 1995;270(35):20775-20780.
27. Kuusanmäki H, Dufva O, Vähä-Koskela M, et al. Erythroid/megakaryocytic differentiation confers BCL-XL dependency and venetoclax resistance in acute myeloid leukemia. Blood. 2023;141(13):1610-1625.
28. van Galen P, Hovestadt V, Wadsworth Ii MH, et al. Single-Cell RNA-Seq Reveals AML Hierarchies Relevant to Disease Progression and Immunity. Cell. 2019;176(6):1265-1281.e1224.
29. Mandai M, Hamanishi J, Abiko K, Matsumura N, Baba T, Konishi I. Dual Faces of IFNγ in Cancer Progression: A Role of PD-L1 Induction in the Determination of Pro- and Antitumor Immunity. Clin Cancer Res. 2016;22(10):2329-2334.
30. Beziaud L, Young CM, Alonso AM, Norkin M, Minafra AR, Huelsken J. IFNγ-induced stem-like state of cancer cells as a driver of metastatic progression following immunotherapy. Cell Stem Cell. 2023;30(6):818-831.e816.
31. Iacobucci I, Wen J, Meggendorfer M, et al. Genomic subtyping and therapeutic targeting of acute erythroleukemia. Nat Genet. 2019;51(4):694-704.

32. Iacobucci I, Qu C, Varotto E, et al. Modeling and targeting of erythroleukemia by hematopoietic genome editing. Blood. 2021;137(12):1628-1640.
33. Takeda J, Yoshida K, Nakagawa MM, et al. Amplified EPOR/JAK2 Genes Define a Unique Subtype of Acute Erythroid Leukemia. Blood Cancer Discov. 2022;3(5):410-427.
34. Gera K, Martir D, Xue W, Wingard JR. Survival after Pure (Acute) Erythroid Leukemia in the United States: A SEER-Based Study. Cancers (Basel). 2023;15(15):3941.
35. Boddu P, Benton CB, Wang W, Borthakur G, Khoury JD, Pemmaraju N. Erythroleukemia-historical perspectives and recent advances in diagnosis and management. Blood Rev. 2018;32(2):96-105.
36. Takeda J. [Molecular pathogenesis and therapeutic targets in acute erythroid leukemia]. Rinsho Ketsueki. 2022;63(2):121-133.
37. Del Prete A, Martínez-Muñoz L, Mazzon C, et al. The atypical receptor CCRL2 is required for CXCR2-dependent neutrophil recruitment and tissue damage. Blood. 2017;130(10):1223-1234.
38. Marki A, Ley K. Leaking chemokines confuse neutrophils. J Clin Invest. 2020;130(5):2177-2179.
39. Stengel A, Meggendorfer M, Walter W, et al. Interplay of TP53 allelic state, blast count, and complex karyotype on survival of patients with AML and MDS. Blood Adv. 2023;7(18):5540-5548.
40. Ramana CV, Gil MP, Schreiber RD, Stark GR. Stat1-dependent and -independent pathways in IFN-gamma-dependent signaling. Trends Immunol. 2002;23(2):96-101.
41. Li L, Muftuoglu M, Ayoub E, et al. TP53 Mutations within T Cells Induce T-Cell Exhaustion and Functional Impairment in TP53 Mutant AML. Blood. 2024;144(Supplement 1):330.
42. Xie X, Zhang W, Zhou X, et al. Low doses of IFN-γ maintain self-renewal of leukemia stem cells in acute myeloid leukemia. Oncogene. 2023;42(50):3657-3669.
43. Hughes CS, Moggridge S, Müller T, Sorensen PH, Morin GB, Krijgsveld J. Single-pot, solid-phase-enhanced sample preparation for proteomics experiments. Nat Protoc. 2019;14(1):68-85.
44. Wang Y, Yang F, Gritsenko MA, et al. Reversed-phase chromatography with multiple fraction concatenation strategy for proteome profiling of human MCF10A cells. Proteomics. 2011;11(10):2019-2026.
45. Larsen MR, Thingholm TE, Jensen ON, Roepstorff P, Jørgensen TJ. Highly selective enrichment of phosphorylated peptides from peptide mixtures using titanium dioxide microcolumns. Mol Cell Proteomics. 2005;4(7):873-886.
46. Herbrich SM, Cole RN, West KP Jr., et al. Statistical inference from multiple iTRAQ experiments without using common reference standards. J Proteome Res. 2013;12(2):594-604.
47. Chang YT, Hernandez D, Alonso S, et al. Role of CYP3A4 in bone marrow microenvironment-mediated protection of FLT3/ITD AML from tyrosine kinase inhibitors. Blood Adv. 2019;3(6):908-916.
48. Hung SC, Pochampally RR, Chen SC, Hsu SC, Prockop DJ. Angiogenic effects of human multipotent stromal cell conditioned medium activate the PI3K-Akt pathway in

hypoxic endothelial cells to inhibit apoptosis, increase survival, and stimulate angiogenesis. Stem Cells. 2007;25(9):2363-2370.
49. Gao J, Aksoy BA, Dogrusoz U, et al. Integrative analysis of complex cancer genomics and clinical profiles using the cBioPortal. Sci Signal. 2013;6(269):pl1.
50. Cerami E, Gao J, Dogrusoz U, et al. The cBio cancer genomics portal: an open platform for exploring multidimensional cancer genomics data. Cancer Discov. 2012;2(5):401-404.
51. Weinstein JN, Collisson EA, Mills GB, et al. The Cancer Genome Atlas Pan-Cancer analysis project. Nat Genet. 2013;45(10):1113-1120.

Figure legends

Fig. 1. CCRL2 is upregulated in *TP53*-mutated MDS/AML and erythroleukemia. (A) Comparison of CCRL2 expression between different AML subtypes based on data extracted from the TCGA dataset. AML M6 and M7 subtypes, respectively, expressed higher levels of *CCRL2* compared to other AML subtypes based on RNA-Seq by Expectation-Maximization (RSEM) ($p<0.01$). **(B)** Comparison of the expression of *CCRL2* in AML samples based on Beat AML dataset showed that *TP53* mutated (MT) AMLs have higher *CCRL2* expression compared to wildtype (WT) ones ($p=0.015$) and healthy ones ($p<0.001$). **(C)** Comparison of CCRL2 expression in different AML cell lines based on differentiation was performed using data from DepMap Portal. AML cell lines with erythroid and megakaryocytic (EM) differentiation have higher expression of *CCRL2* than AML cell lines with no EM differentiation($p<0.001$). **(D)** CCRL2 expression was compared in blasts from acute erythroid leukemia (AEL) patients ($p<0.001$) and *TP53* MT MDS/AML patients ($p=0.008$) to healthy controls **(E)** CD34+ cells from acute erythroid leukemia AEL patients ($p<0.001$) and *TP53* MT MDS/AML patients ($p=0.005$) have higher CCRL2 expression compared to healthy controls and CD34+ cells from acute erythroid leukemia (AEL) patients have higher CCRL2 expression than those from *TP53* MT MDS/AML patients($p<0.001$). **(F)** Flow cytometry showing CCRL2 expression in blasts and CD34+ cells from representative samples of healthy donors, *TP53* MT MDS/AML, and acute erythroid leukemia (AEL). **(G)** *TP53* knockout (KO) UKE-1 cells showed higher CCRL2 expression at the protein level compared to *TP53* WT UKE-1 cells ($p<0.001$). **(H)** Analysis of RNA-seq data (GSE180851) showed a gradual increase in CCRL2 expression in

megakaryocytic-erythroid progenitor (MEP) cells associated with *Trp53* loss (from *Jak2*^{mut} to *Jak2*^{mut}*Trp53*+/- and *Jak2*^{mut}*Trp53*-/-) compared to wild type (WT) MEPs.

Fig. 2. CCRL2 promotes the clonogenicity of erythroleukemia cells *in vitro* and the growth of erythroleukemia in mice. (A-B) CCRL2 KO with two different sgRNAs decreases the colony formation of the granulocyte-macrophage colony-stimulating factor (GM-CSF) dependent TF-1 and F36P cells in the absence and presence of GM-CSF. **(C-E)** CCRL2 KO with two different sgRNAs decreases the colony formation of K562, SET2, and HEL cells. **(F, G)** TF-1 cells with WT (sgControl) or KO (sgCCRL2) CCRL2 were transduced with a GFP+/Luciferase dual reporter retrovirus and injected into NSG mice. At day 50 after injection, the bioluminescence signal in mice injected with CCRL2 KO was significantly lower (p=0.021). **(H)** Mice engrafted with sgControl cells had a significantly poorer overall survival than those engrafted with sgCCRL2 (p=0.002). **(I, J)** SET2 cells with WT (sgControl) or KO (sgCCRL2) CCRL2 were transduced with a GFP+/Luciferase dual reporter retrovirus and injected into NSG mice. At day 60 after injection, the bioluminescence signal in mice injected with suppressed CCRL2 was significantly lower (p=0.04). **(K)** There was no significant difference in the survival in mice engrafted with SET2 sgControl cells compared to mice engrafted with sgCCRL2.

Fig. 3. CCRL2 promotes IFN-γ response signaling in erythroleukemia cells (A) Pathway enrichment analysis of phospho-proteomic data was performed to identify the pathways affected more prominently by CCRL2 KO at the protein level in TF-1 cells. Interferon (IFN) signaling was identified as the top pathway downregulated by CCRL2 KO, and Liver X Receptor-Retinoid X Receptor (LXR/RXR) pathway was the top pathway upregulated by CCRL2 KO. **(B)**

Heatmap, including the top CCRL2 associated genes represented in the volcano plot in addition to other various IFN-γ/STAT1 targets, shows that these targets are significantly downregulated by TF-1 CCRL2 KO. MS represents mean subtracted values. The intensity scale to the right shows a range of values from -1.709 to 1.151, with the blue color representing the lower extreme values of this range and red color representing the high extreme values of the range. **(C)** IFN-γ signaling was found to be the top CCRL2-regulated pathway by gene set enrichment analysis of RNA-seq data in SET2 cells transduced with sgControl or sgCCRL2 (CCRL2 KO). **(D)** Heatmap shows that CCRL2 regulated IFN-γ/STAT1 associated genes, are significantly downregulated by SET2 CCRL2 KO. The intensity scale to the right shows a range of values from 0.85 to 1, with the blue color representing the lower extreme values of this range and the red color representing the high extreme values of the range.

Fig. 4. CCRL2 induces STAT1 phosphorylation partially via JAK2.

(A) Western blotting was performed to analyze two sites of STAT1 phosphorylation: tyrosine 701 (Y701) phosphorylation and serine 727 (S727) phosphorylation. CCRL2 KO suppressed STAT1 Y701 phosphorylation in TF-1 and had a less prominent effect on STAT1 S727 phosphorylation. **(B)** Similarly, CCRL2 KO suppressed STAT1 Y701 phosphorylation in F36P cells. No S727 phosphorylation was detected in F36P cells, and no STAT1 phosphorylation was detected in the absence of GM-CSF. **(C)** STAT1 Y701 phosphorylation was suppressed in SET2 CCRL2 KO cells with a milder effect on S727 phosphorylation. **(D)** Quantitative real-time PCR demonstrated that CCRL2 KO suppresses the RNA levels of 3 representative IFN-γ/STAT1 target genes, namely *IFIT3*, *IFI30* and *MT2A* in TF-1 and SET2 cells compared to WT cells. **(E)** Treatment of iCCRL2 TF-1 cells with 10 ng/ml doxycycline induced STAT1 Y701 and S727 phosphorylation; however, concurrent treatment with fedratinib suppressed Y701 but not S727

phosphorylation. **(F)** Co-immunoprecipitation assay showing that CCRL2 KO decreases the precipitation of STAT1 with an anti-JAK2 antibody in TF-1, F36P cells, and SET2 while induction of CCRL2 by 10 ng/ml doxycycline increases STAT1 precipitation in iCCRL2 TF-1 cells.

Fig. 5. CCRL2/IFN-γ signaling is upregulated in AML with erythroid differentiation and *TP53* mutations without an increase in IFN-γ secretion

(A) Based on data derived from TCGA, an overall score for 18 genes involved in CCRL2/IFN-γ signaling was calculated. AML with erythroid and megakaryocytic (EM) differentiation (AML M6 and M7 subtypes, respectively) expressed higher levels of the CCRL2/IFN signaling score ($p=0.06$) compared to other subtypes of AML. **(B)** Analysis of DepMap Portal data showed that erythroid cell lines had higher CCRL2/IFN-γ signaling score than other AML cell lines ($p=0.02$). (**C)** Analysis of Beat AML data demonstrated that AML with *TP53* mutation (MT) had a higher CCRL2/IFN-γ signaling score compared to *TP53* wildtype (WT) AML ($p=0.03$). CCRL2/IFN-γ signaling score was also higher in *TP53* WT AML than healthy CD34+ controls($p<0.0001$). **(D)** Based on publicly available single-cell RNA sequencing data, clustering of AML blasts and monocytes from 5 patients with different AML subtypes was performed based on differentiation. **(E)** The AML patient (AML5- Erythroid) with erythroid differentiation had upregulated expression of *IFIT1* (average log2 fold change = 4.98; adjusted $p < 0.0001$); *ISG15* (average log2 fold change = 3.80; adjusted $p < 0.0001$); and *IFIT3* (avg log2 fold change = 3.37; adjusted $p < 0.0001$) compared to the other AML patients. **(F)** Specifically**,** *IFIT3, IFIH1* and *IFITM3* are significantly upregulated in blasts from *TP53* mutated AML samples (p adjusted= 6.712E-07,

0.0005 and 0.024 respectively) compared to blasts from *TP53* WT AML patients, as shown in the Gene expression BoxPlot. Each dot in the boxplot represents the pseudobulk aggregated expression data for one study participant normalized by a size factor as implemented in DESeq2**.** **(G)** *TP53* KO in UKE-1 cells led to a prominent increase in both Y701 and S727 phosphorylation of STAT1 compared to *TP53* WT UKE-1 cells. **(H)** *IFIT3* is upregulated in *TP53* KO UKE1 cells compared to *TP53* WT UKE-1 cells (p=0.016 with KO1 and p=0.002 with KO2).

Fig. 6. CCRL2/IFN-γ signaling upregulation is associated with selection of *TP53* mutated clones

(A) Analysis of DepMap portal publicly available CRISPR-Cas9 dataset showed that most CCRL2/IFN-γ target genes exhibit a negative gene effect in AML cell lines with erythroid differentiation and *TP53* mutations (HEL, HEL9217, SET2, TF-1, CMK115, MUTZ8, OCIM2 and F36P) (**B)** Treatment of primary AML blasts from 3 independent *TP53* mutated AML patients with 10 ng/ml and 20 ng/ml of IFN-γ for 72 hours induced apoptosis of leukemic blasts (p=0.010 and p=0.007 respectively) and decreased the percentage of CD34+CD117+ cells (p<0.001 for both doses). **(C)** Volcano plot showed that a significant subset of CCRL2/IFN-γ associated genes is upregulated in pre-leukemic *TP53* heterozygous clones from myeloproliferative neoplasms (MPN) patients who transformed to sAML compared to those who remained in CP-MPN.

Fig.7 CCRL2/IFN-γ signaling upregulation is associated with AML resistance to venetoclax

(A) Analysis of data from Beat AML dataset showed that CCRL2/IFN-γ signaling score is positively correlated with venetoclax IC50 ($p<0.0001$). Patients in cluster 2 who had a high expression of *IFIT2, IFIT1, IFIT3, STAT1, IFI6, IFIH1, ISG15,* and *IRF7* had significantly higher Venetoclax IC50 values compared to cluster 1 patients ($p<0.001$). (**B-C**) TF-1 and F36P CCRL2 KO cells treated with increasing doses of venetoclax (μM) have increased sensitivity to venetoclax compared to TF-1 and F36P CCRL2 WT cells. IC50= 5.67 μM in TF-1 CCRL2 WT and IC50= 3.48 μM and 3.4 uM in TF-1 KO1 (sgCCRL2-1) and KO2 (sgCCRL2-2) respectively and IC50= 8.93 μM in F36P CCRL2 WT compared to IC50= 4.4 μM and 2.3 μM in KO1 (sgCCRL2-1) and KO2 (sgCCRL2-2). **(D)** Based on data from Beat AML dataset, patients with high CCRL2/IFN-γ signaling score (red) had a worse overall survival compared to patients with low CCRL2/IFN-γ signaling score (gray) over 100 months. **(E)** *TP53* deletion/loss of function promotes CCRL2/IFN-γ signaling response in AML subtypes, which appears to be associated with a cell-intrinsic effect independent of IFN-γ levels in the microenvironment, and the latter is associated with selection of *TP53* mutated pre-leukemic clones, resistance to venetoclax and poor overall survival.

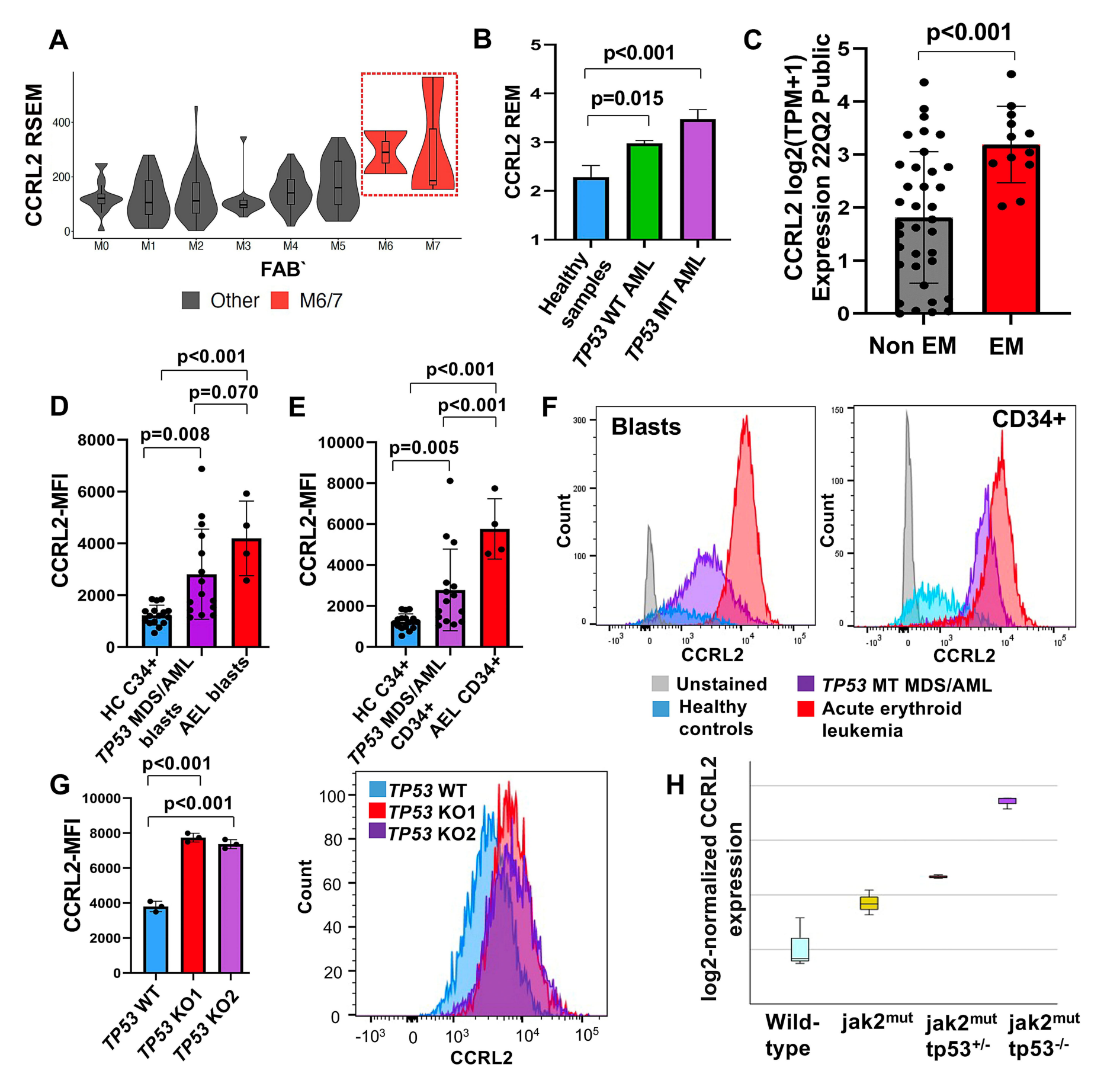
A
CCRL2 RSEM
400
200
0
M0
M1
M2
M3
M4
M5
M6
M7
FAB`
Other
M6/7
B
CCRL2 REM
p<0.001
p=0.015
Healthy samples
TP53 WT AML
TP53 MT AML
C
CCRL2 log2(TPM+1) Expression 22Q2 Public
p<0.001
Non EM
EM
D
CCRL2-MFI
p<0.001
p=0.070
p=0.008
HC C34+
TP53 MDS/AML blasts
AEL blasts
E
CCRL2-MFI
p<0.001
p<0.001
p=0.005
HC C34+
TP53 MDS/AML CD34+
AEL CD34+
F
Blasts
CD34+
Count
CCRL2
Unstained
Healthy controls
TP53 MT MDS/AML
Acute erythroid leukemia
G
CCRL2-MFI
p<0.001
p<0.001
TP53 WT
TP53 KO1
TP53 KO2
TP53 WT
TP53 KO1
TP53 KO2
Count
CCRL2
H
log2-normalized CCRL2 expression
Wild-type
jak2mut
jak2mut tp53+/-
jak2mut tp53-/-

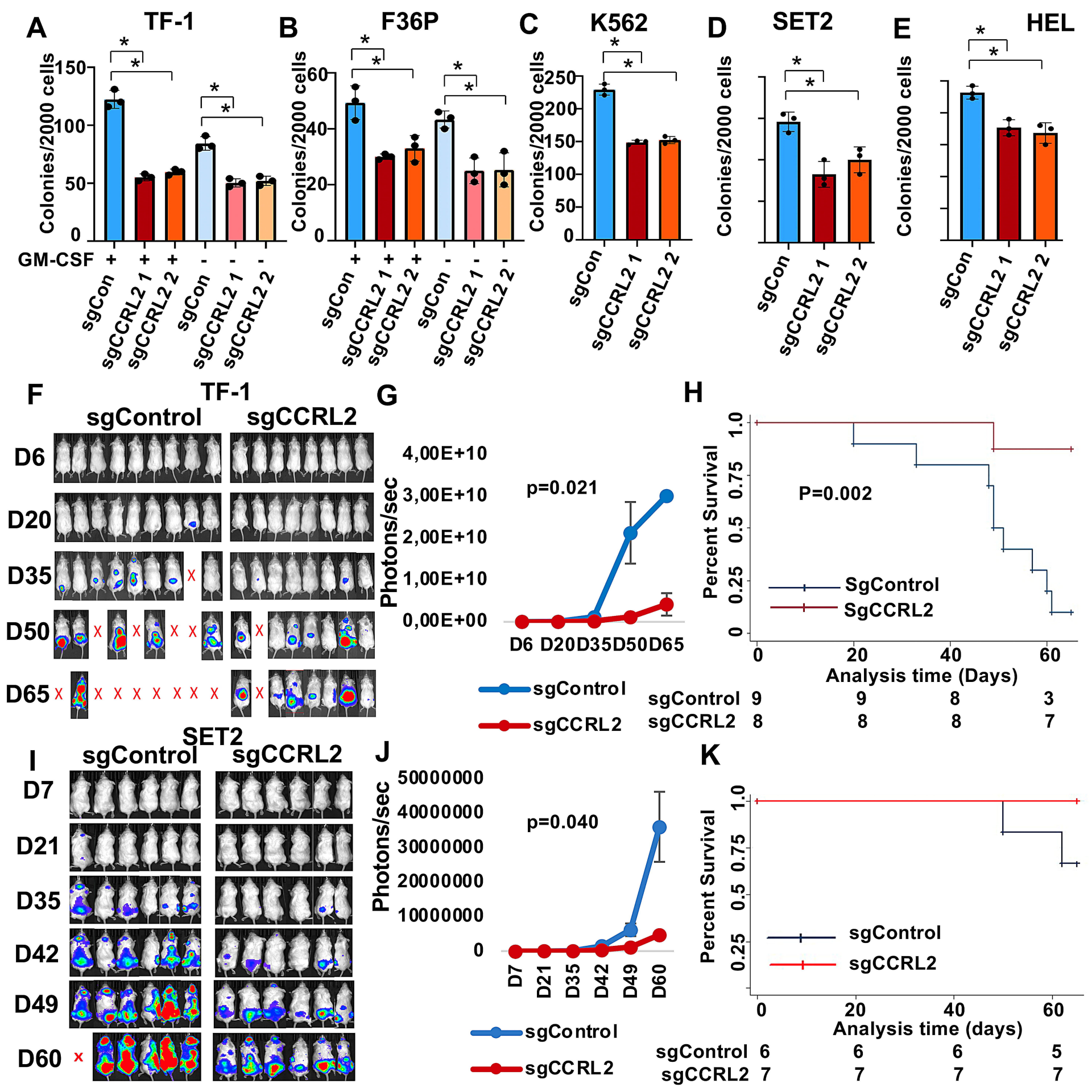
A
TF-1
B
F36P
C
K562
D
SET2
E
HEL
Colonies/2000 cells
GM-CSF
sgCon
sgCCRL2 1
sgCCRL2 2
F
TF-1
sgControl
sgCCRL2
D6
D20
D35
D50
D65
G
Photons/sec
p=0.021
sgControl
sgCCRL2
H
Percent Survival
P=0.002
Analysis time (Days)
sgControl 9 9 8 3
sgCCRL2 8 8 8 7
I
SET2
D7
D21
D35
D42
D49
D60
J
p=0.040
K
Analysis time (days)
sgControl 6 6 6 5
sgCCRL2 7 7 7 7

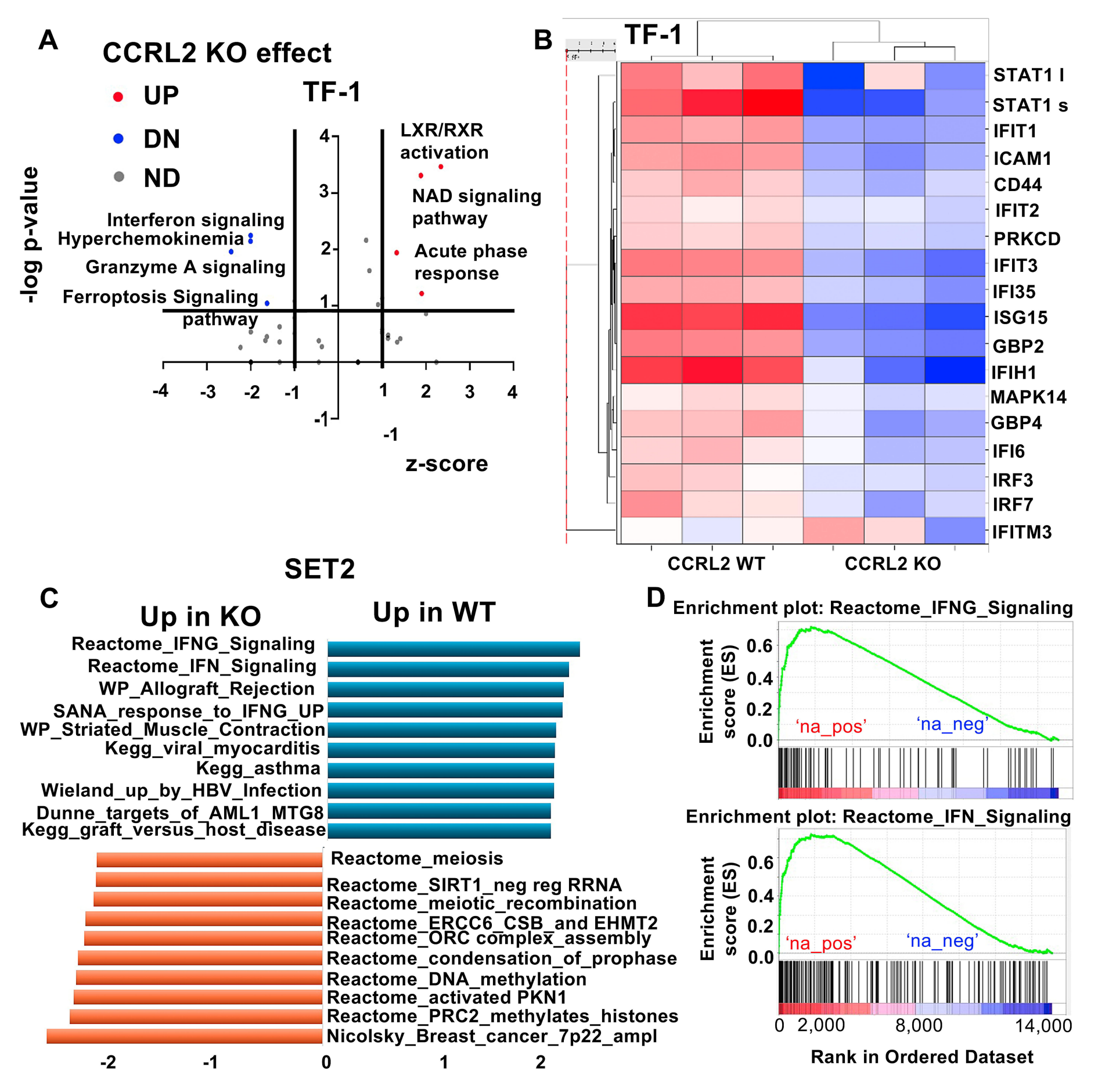
A
CCRL2 KO effect
UP
DN
ND
TF-1
LXR/RXR activation
NAD signaling pathway
Acute phase response
Interferon signaling
Hyperchemokinemia
Granzyme A signaling
Ferroptosis Signaling pathway
-log p-value
z-score
B
TF-1
STAT1 I
STAT1 s
IFIT1
ICAM1
CD44
IFIT2
PRKCD
IFIT3
IFI35
ISG15
GBP2
IFIH1
MAPK14
GBP4
IFI6
IRF3
IRF7
IFITM3
CCRL2 WT
CCRL2 KO
SET2
C
Up in KO
Up in WT
Reactome_IFNG_Signaling
Reactome_IFN_Signaling
WP_Allograft_Rejection
SANA_response_to_IFNG_UP
WP_Striated_Muscle_Contraction
Kegg_viral_myocarditis
Kegg_asthma
Wieland_up_by_HBV_Infection
Dunne_targets_of_AML1_MTG8
Kegg_graft_versus_host_disease
Reactome_meiosis
Reactome_SIRT1_neg reg RRNA
Reactome_meiotic_recombination
Reactome_ERCC6_CSB_and EHMT2
Reactome_ORC complex_assembly
Reactome_condensation_of_prophase
Reactome_DNA_methylation
Reactome_activated PKN1
Reactome_PRC2_methylates_histones
Nicolsky_Breast_cancer_7p22_ampl
D
Enrichment plot: Reactome_IFNG_Signaling
Enrichment score (ES)
'na_pos'
'na_neg'
Enrichment plot: Reactome_IFN_Signaling
Rank in Ordered Dataset

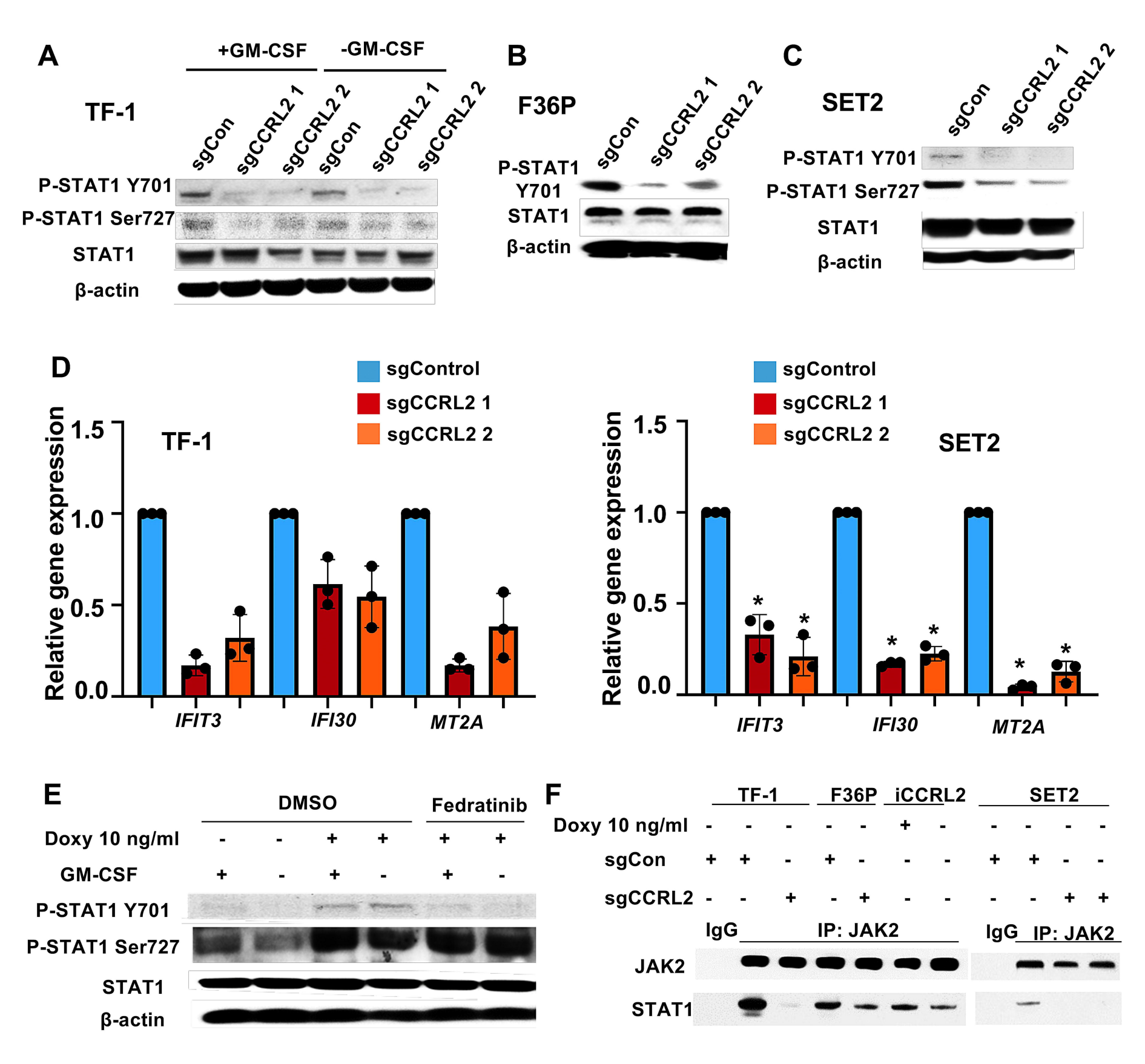
A
+GM-CSF
-GM-CSF
TF-1
sgCon
sgCCRL2 1
sgCCRL2 2
sgCon
sgCCRL2 1
sgCCRL2 2
P-STAT1 Y701
P-STAT1 Ser727
STAT1
β-actin
B
F36P
sgCon
sgCCRL2 1
sgCCRL2 2
P-STAT1 Y701
STAT1
β-actin
C
SET2
sgCon
sgCCRL2 1
sgCCRL2 2
P-STAT1 Y701
P-STAT1 Ser727
STAT1
β-actin
D
sgControl
sgCCRL2 1
sgCCRL2 2
TF-1
Relative gene expression
1.5
1.0
0.5
0.0
IFIT3
IFI30
MT2A
sgControl
sgCCRL2 1
sgCCRL2 2
SET2
Relative gene expression
1.5
1.0
0.5
0.0
*
IFIT3
IFI30
MT2A
E
DMSO
Fedratinib
Doxy 10 ng/ml
GM-CSF
P-STAT1 Y701
P-STAT1 Ser727
STAT1
β-actin
F
TF-1
F36P
iCCRL2
SET2
Doxy 10 ng/ml
sgCon
sgCCRL2
IgG
IP: JAK2
IgG
IP: JAK2
JAK2
STAT1

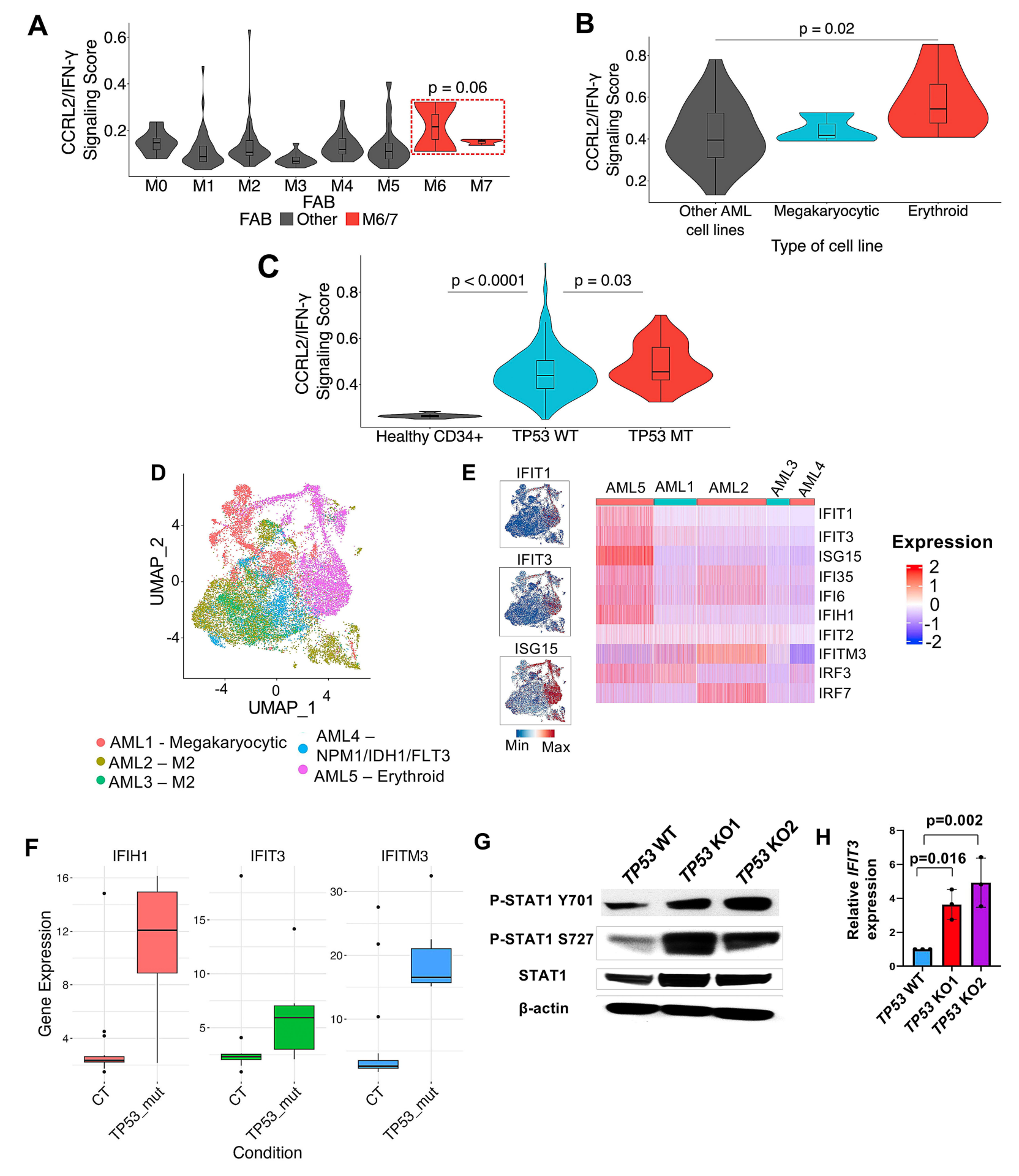
A
CCRL2/IFN-γ Signaling Score
0.6
0.4
0.2
p = 0.06
M0
M1
M2
M3
M4
M5
M6
M7
FAB
FAB Other M6/7
B
p = 0.02
CCRL2/IFN-γ Signaling Score
0.8
0.6
0.4
0.2
Other AML cell lines
Megakaryocytic
Erythroid
Type of cell line
C
CCRL2/IFN-γ Signaling Score
p < 0.0001
p = 0.03
0.8
0.6
0.4
Healthy CD34+
TP53 WT
TP53 MT
D
UMAP_2
4
0
-4
-4
0
4
UMAP_1
AML1 - Megakaryocytic
AML2 – M2
AML3 – M2
AML4 – NPM1/IDH1/FLT3
AML5 – Erythroid
E
IFIT1
IFIT3
ISG15
Min
Max
AML5
AML1
AML2
AML3
AML4
IFIT1
IFIT3
ISG15
IFI35
IFI6
IFIH1
IFIT2
IFITM3
IRF3
IRF7
Expression
2
1
0
-1
-2
F
IFIH1
IFIT3
IFITM3
Gene Expression
16
12
8
4
15
10
5
30
20
10
CT
TP53_mut
Condition
G
TP53 WT
TP53 KO1
TP53 KO2
P-STAT1 Y701
P-STAT1 S727
STAT1
β-actin
H
p=0.002
p=0.016
Relative IFIT3 expression
8
6
4
2
0
TP53 WT
TP53 KO1
TP53 KO2

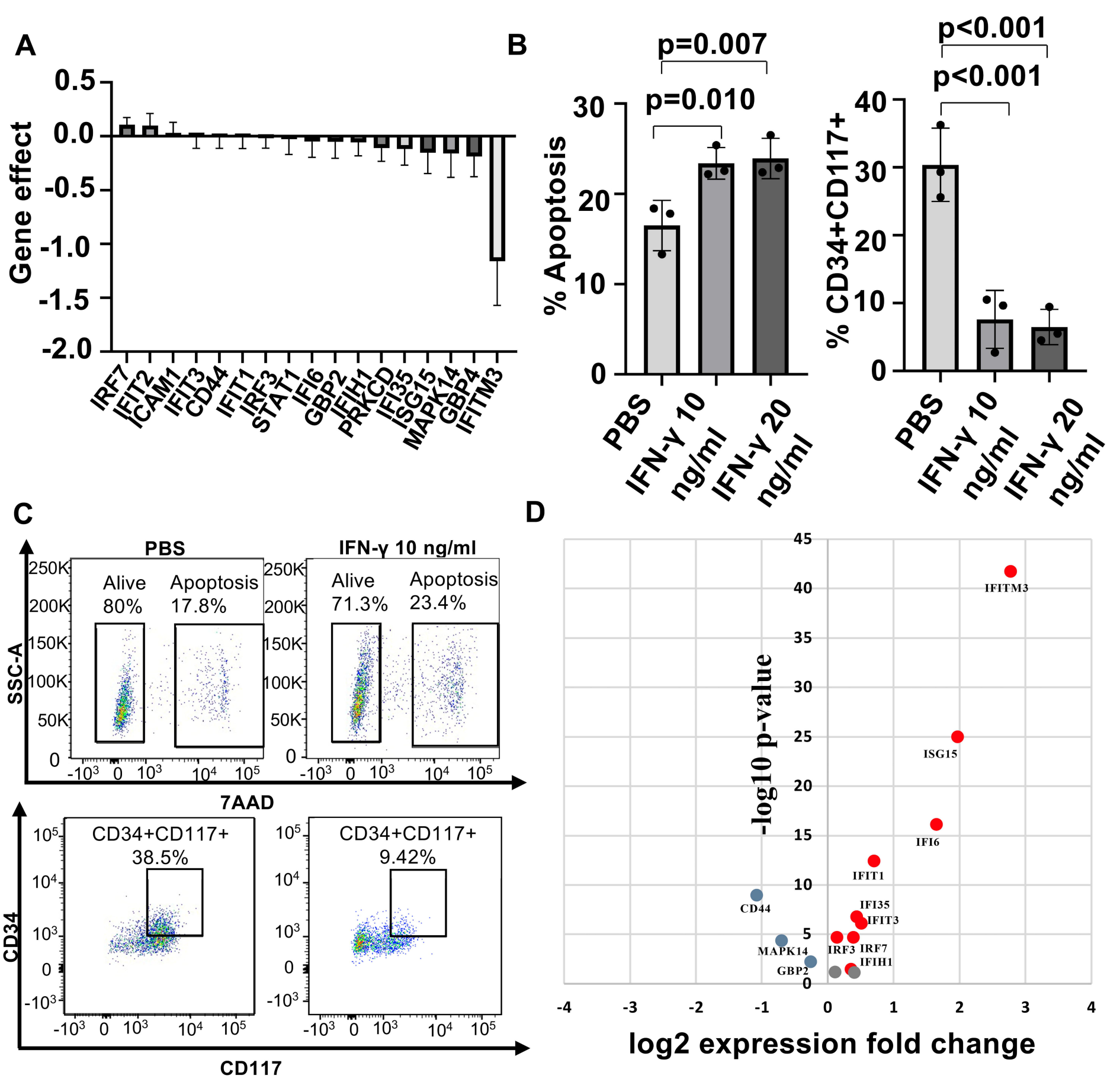
A
Gene effect
0.5
0.0
-0.5
-1.0
-1.5
-2.0
IRF7
IFIT2
ICAM1
IFIT3
CD44
IFIT1
IRF3
STAT1
IFI6
GBP2
IFIH1
PRKCD
IFI35
ISG15
MAPK14
GBP4
IFITM3
B
p=0.007
p=0.010
% Apoptosis
30
20
10
0
PBS
IFN-γ 10 ng/ml
IFN-γ 20 ng/ml
p<0.001
p<0.001
% CD34+CD117+
40
30
20
10
0
PBS
IFN-γ 10 ng/ml
IFN-γ 20 ng/ml
C
PBS
IFN-γ 10 ng/ml
Alive
80%
Apoptosis
17.8%
Alive
71.3%
Apoptosis
23.4%
SSC-A
7AAD
CD34+CD117+
38.5%
CD34+CD117+
9.42%
CD34
CD117
D
-log10 p-value
log2 expression fold change
IFITM3
ISG15
IFI6
IFIT1
IFI35
IFIT3
IRF3
IRF7
IFIH1
CD44
MAPK14
GBP2

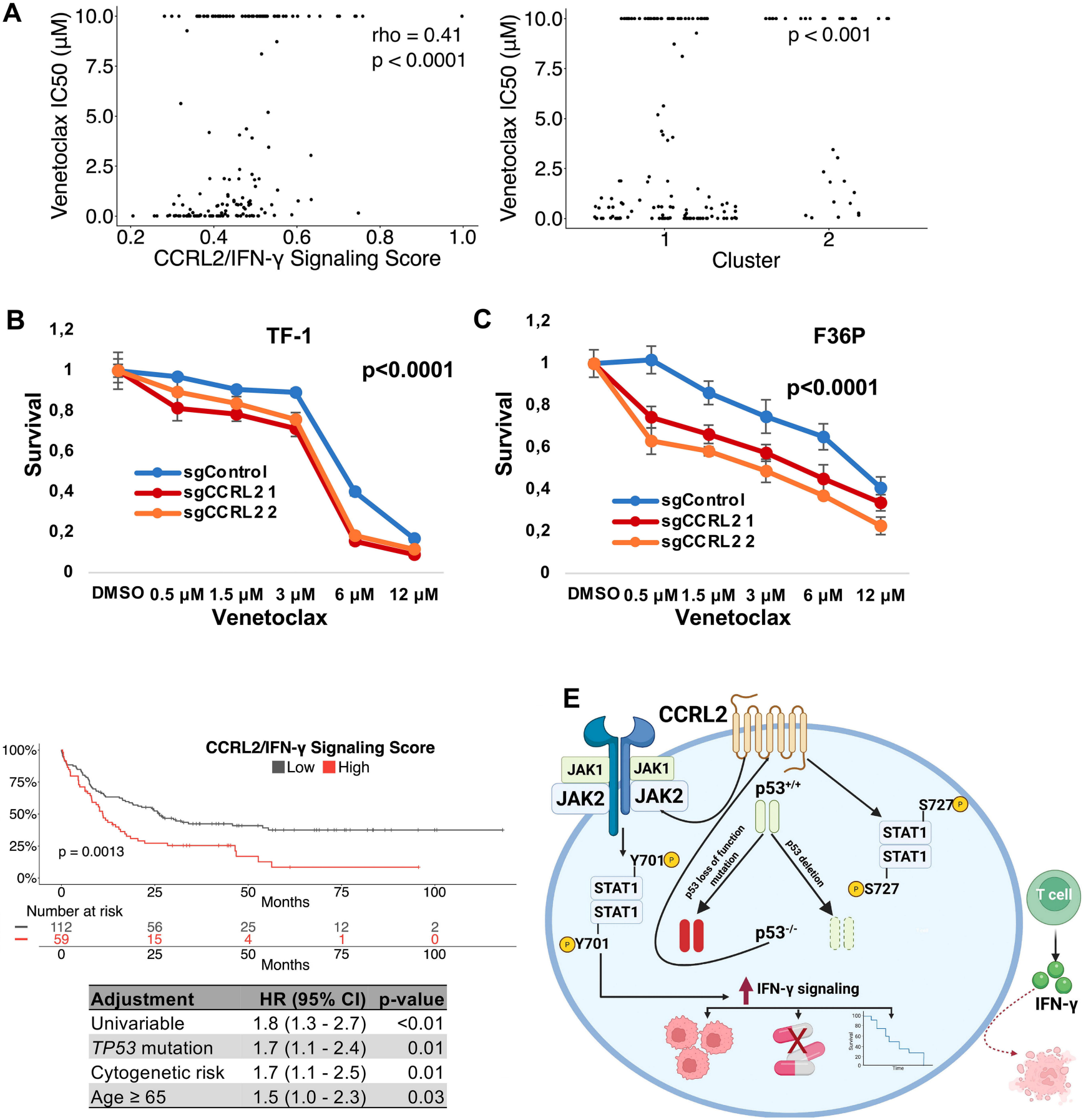

Adjustment	HR (95% CI)	p-value
Univariable	1.8 (1.3 - 2.7)	<0.01
TP53 mutation	1.7 (1.1 - 2.4)	0.01
Cytogenetic risk	1.7 (1.1 - 2.5)	0.01
Age ≥ 65	1.5 (1.0 - 2.3)	0.03

A

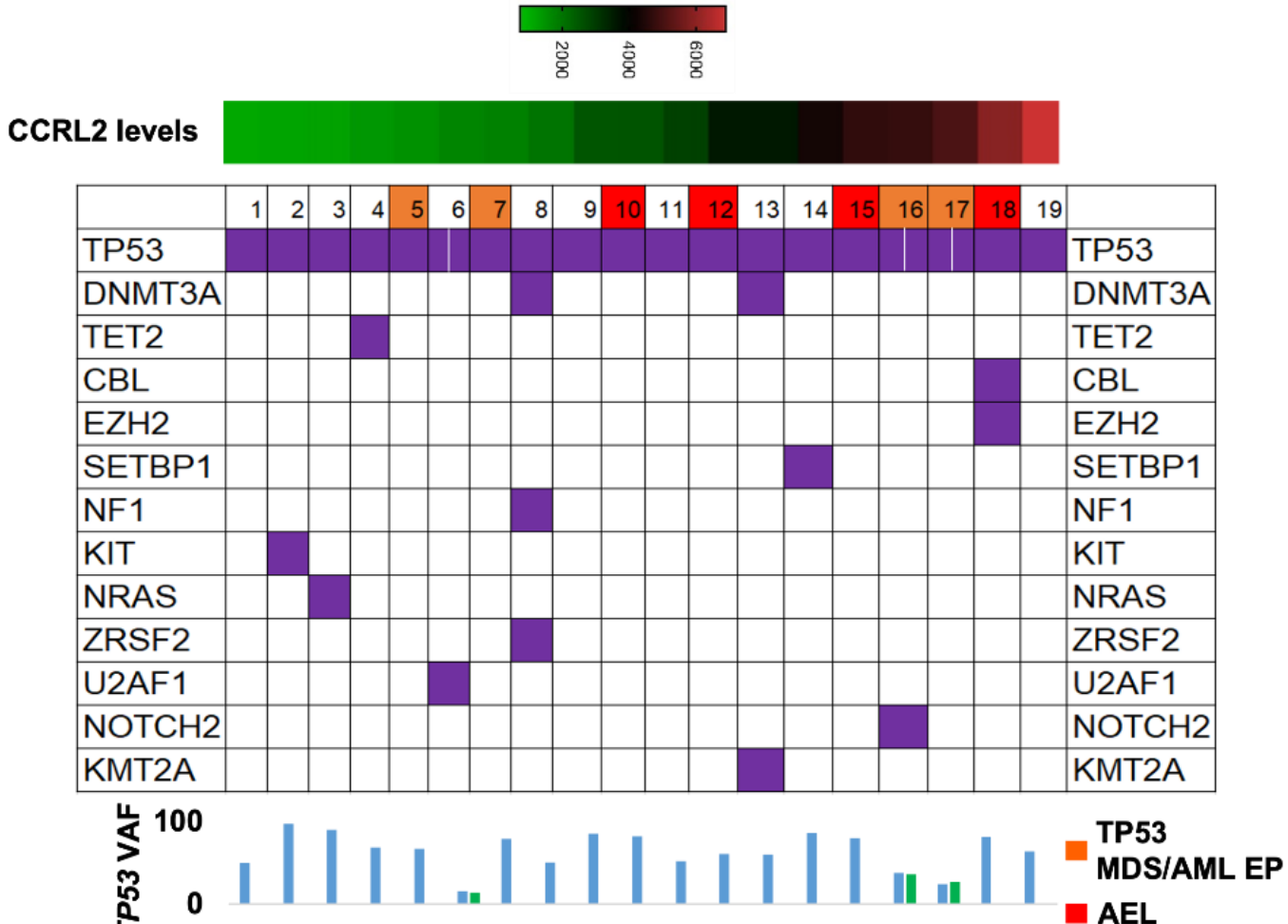

B

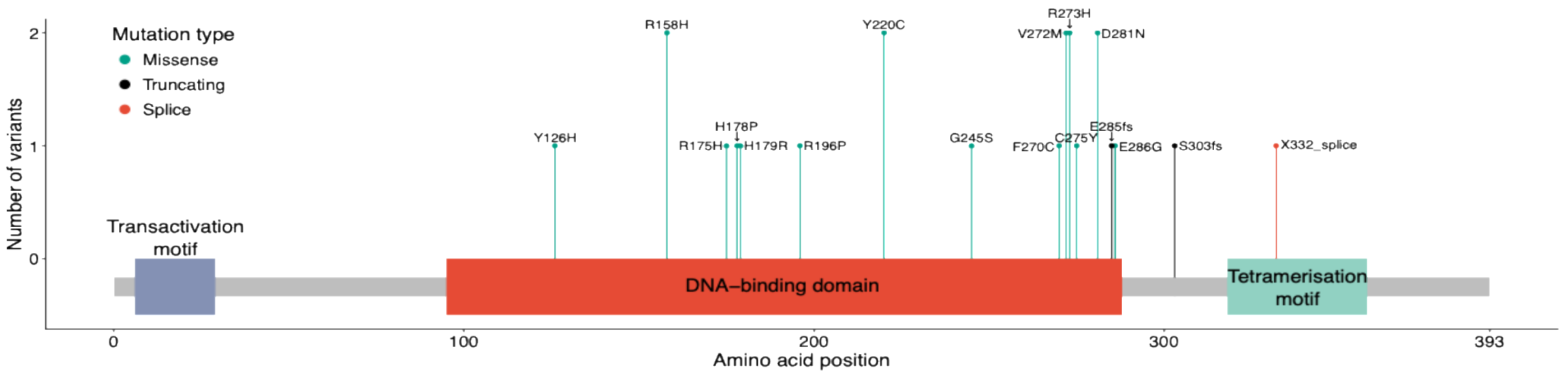

Supplementary Figure 1

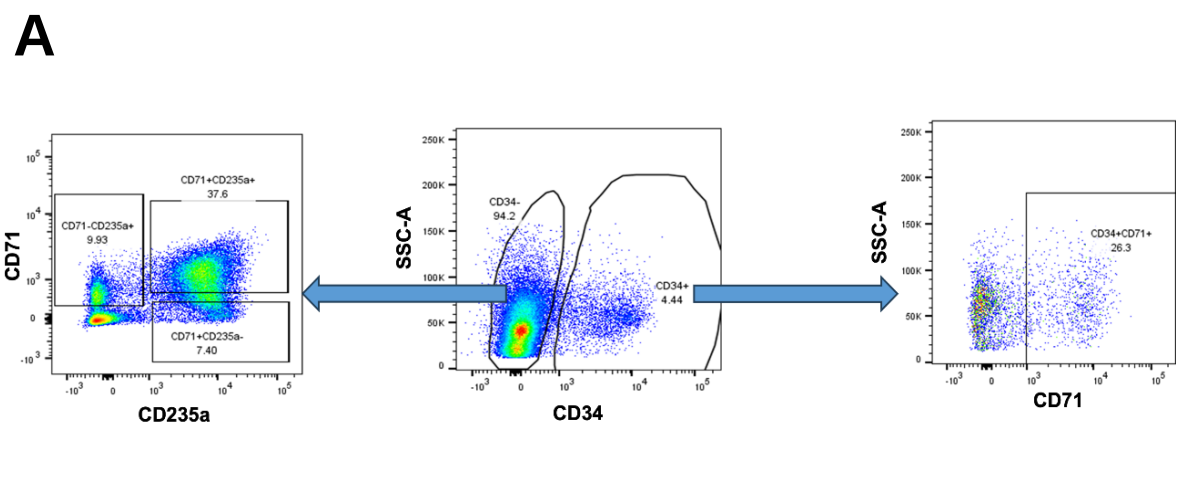

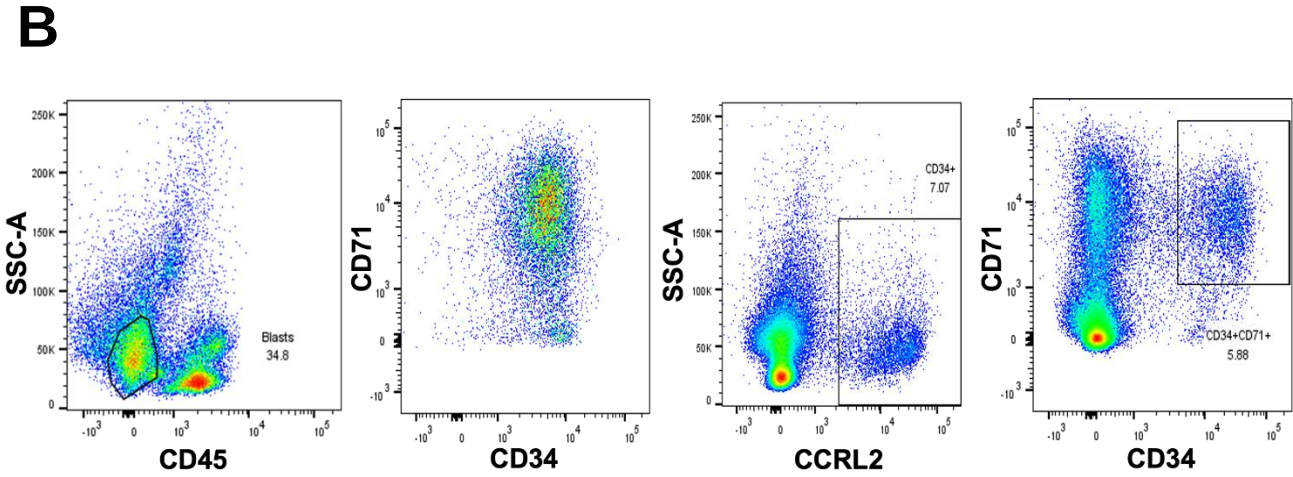

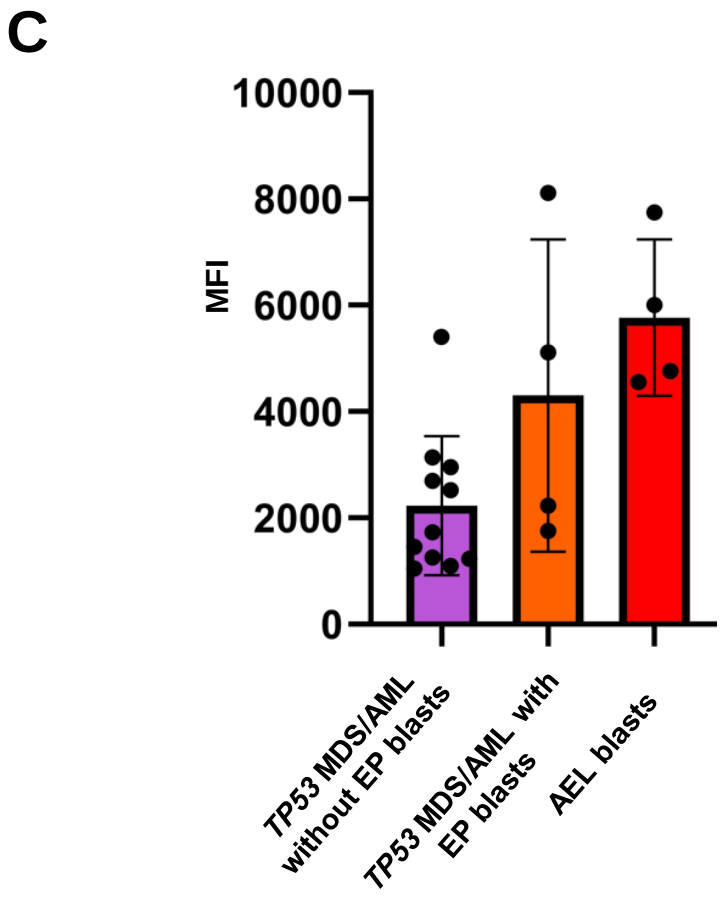

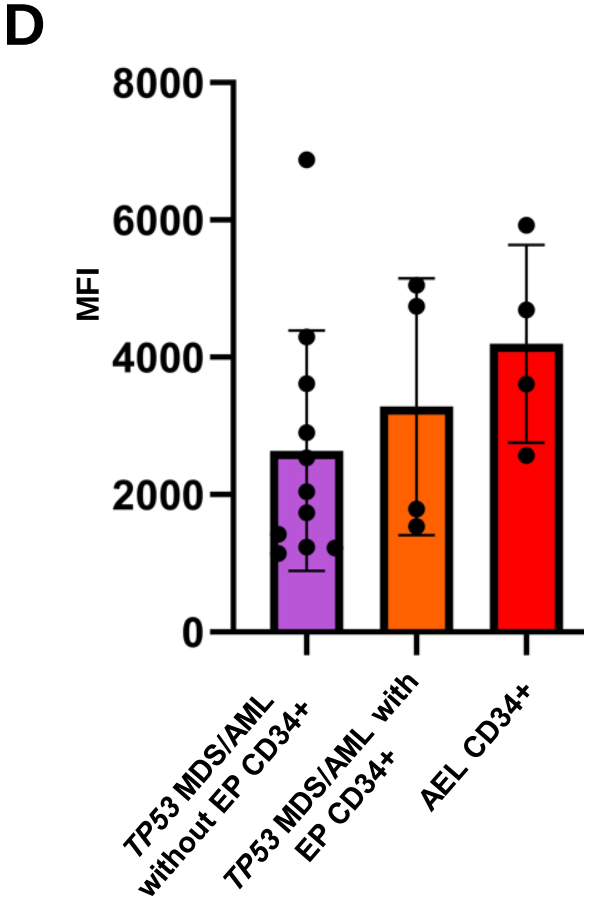

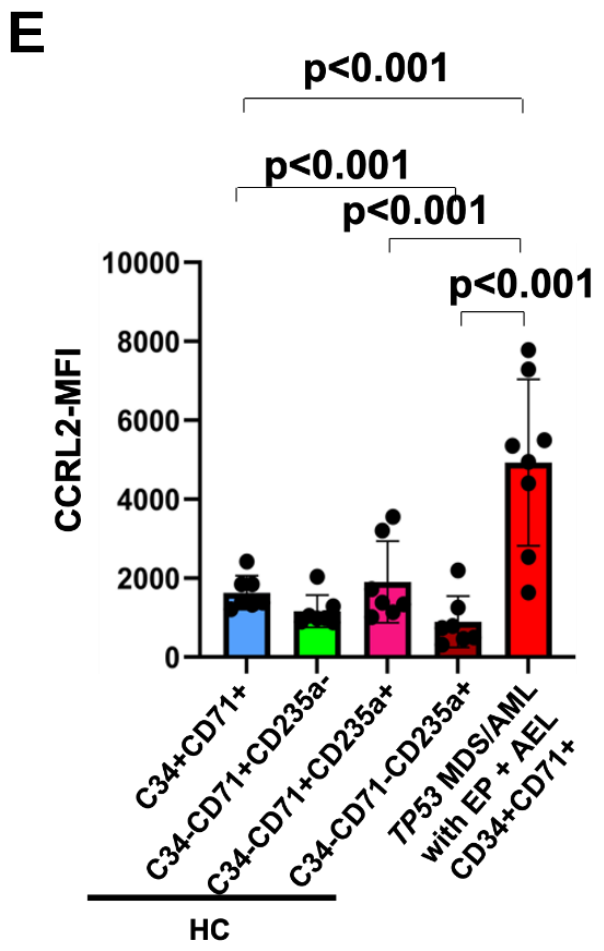

Supplementary Figure 2

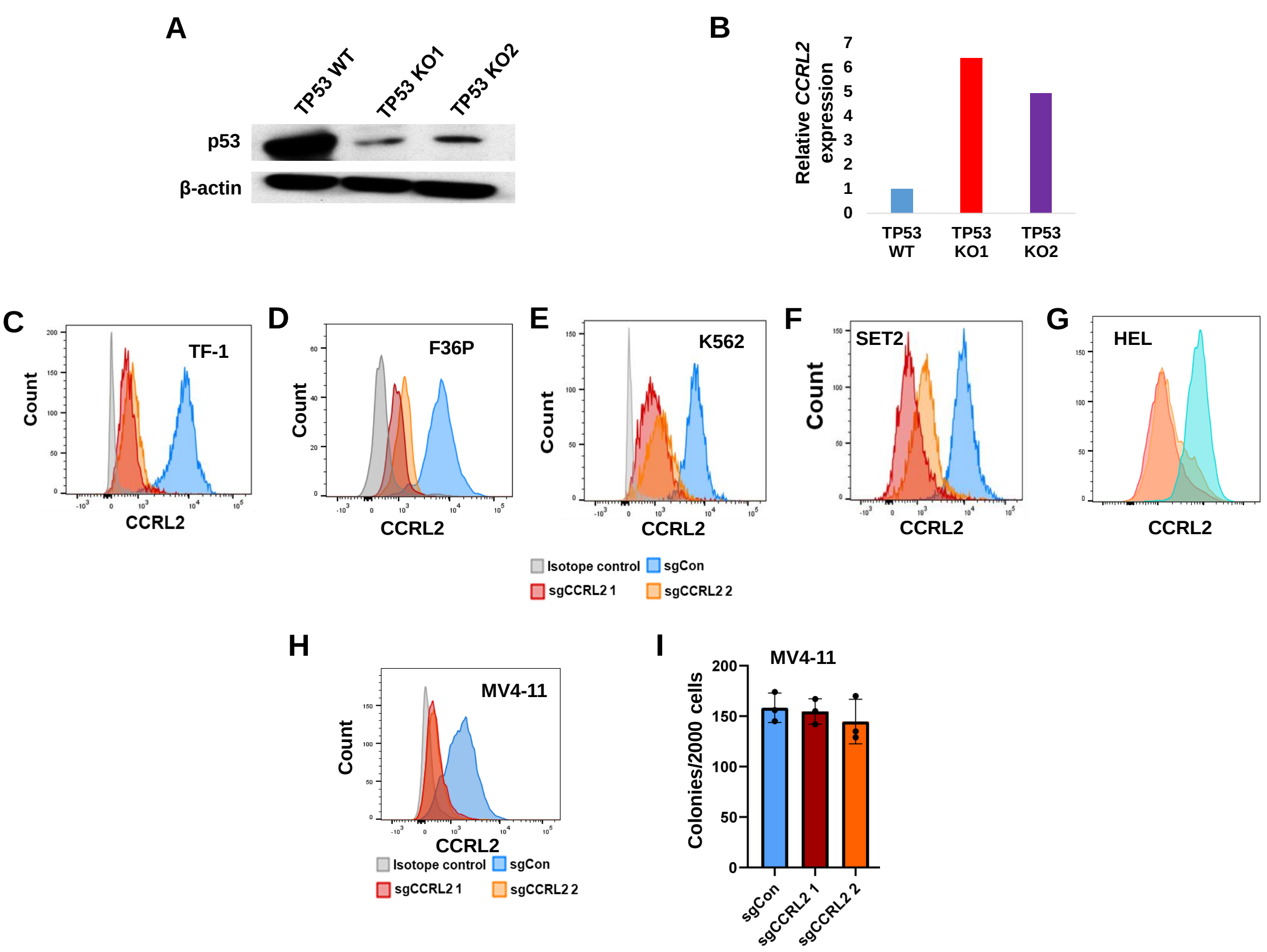

Supplementary Figure 3

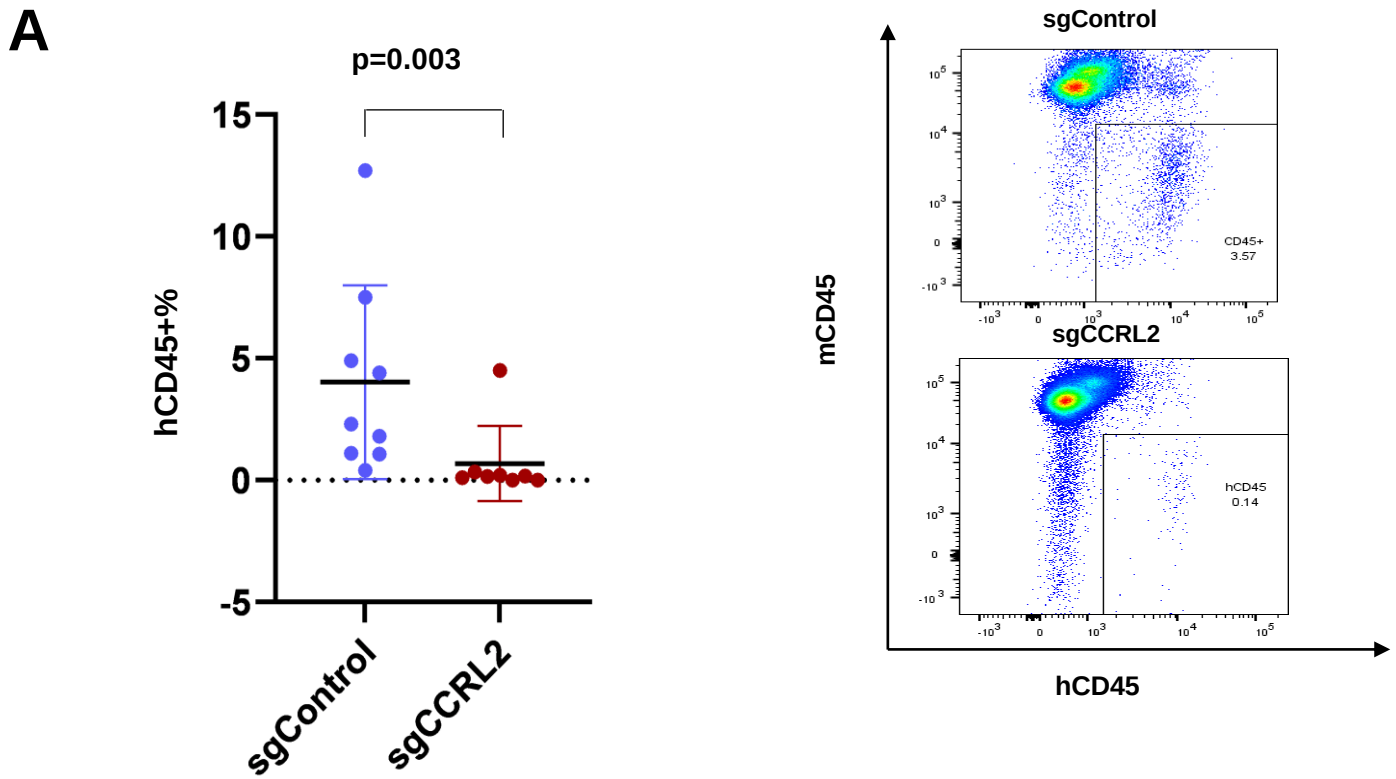

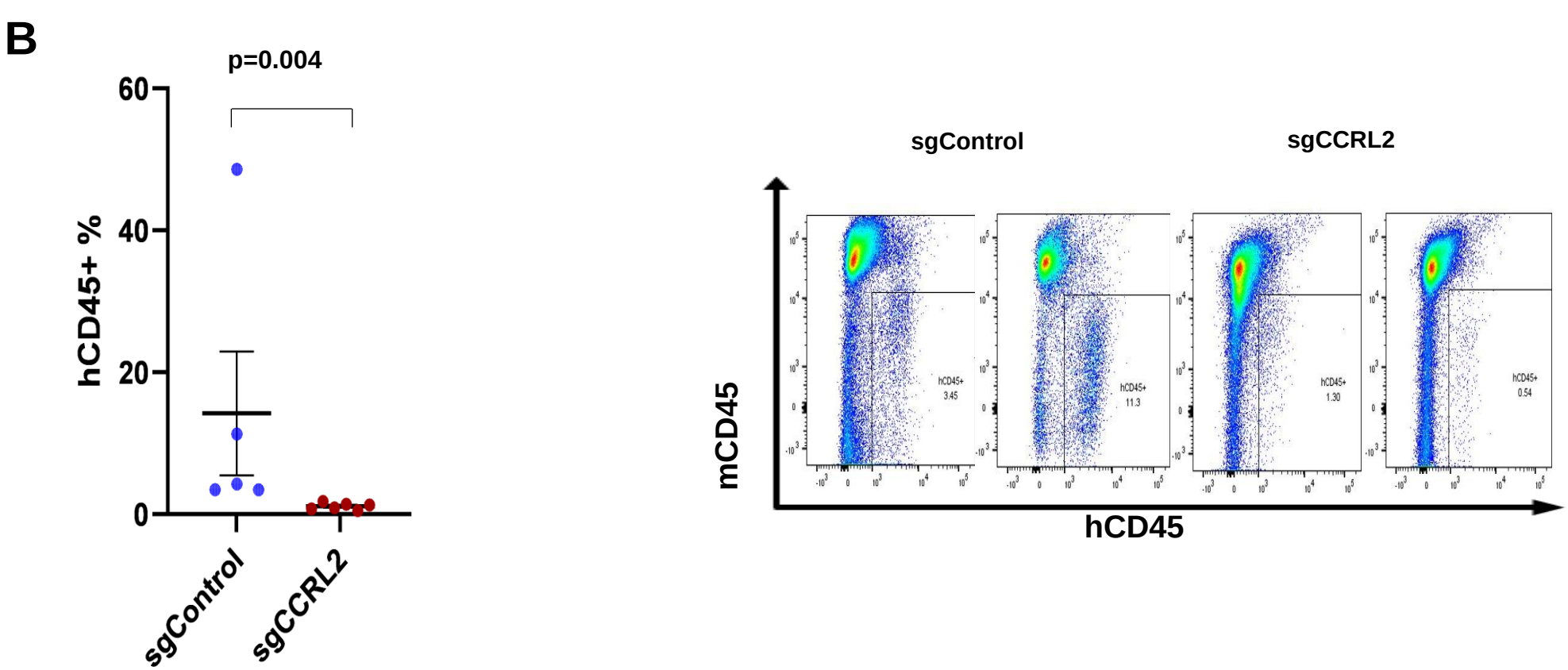

Supplementary Figure 4

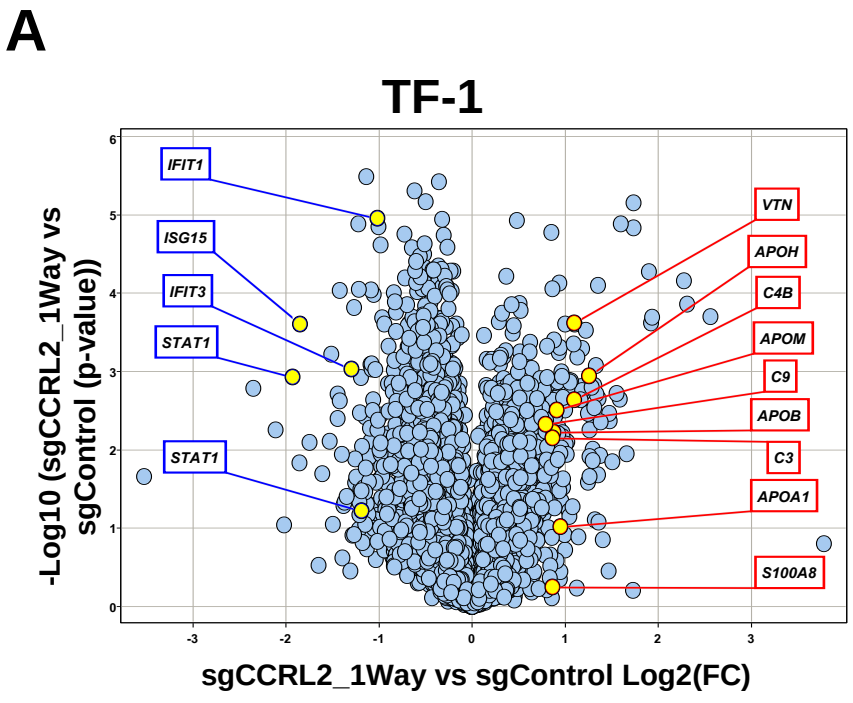

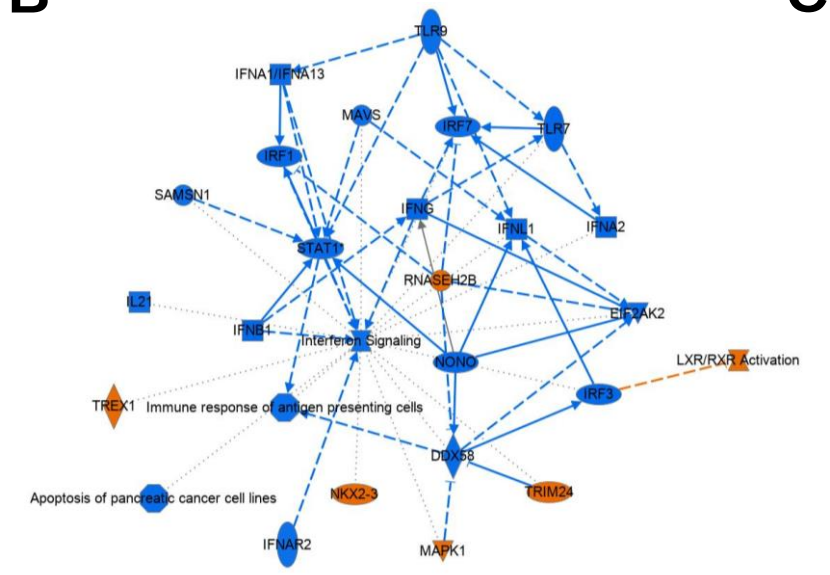

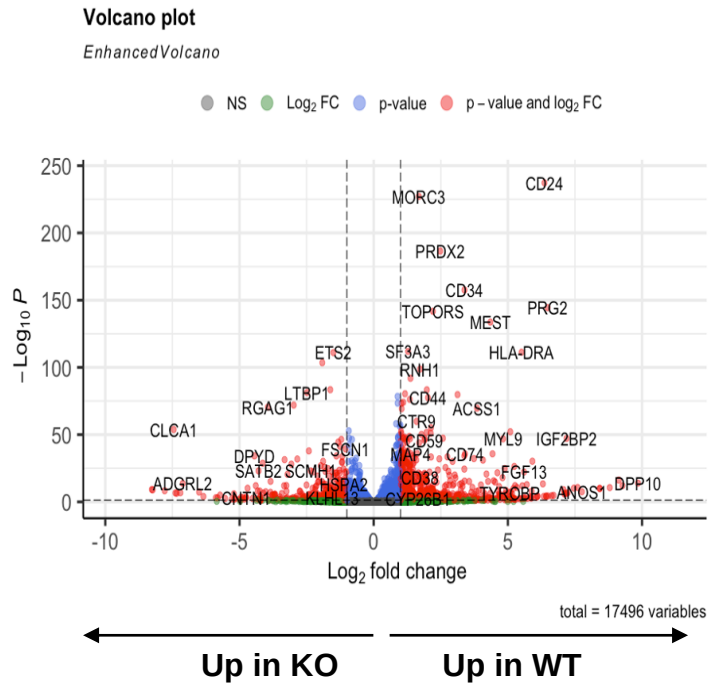

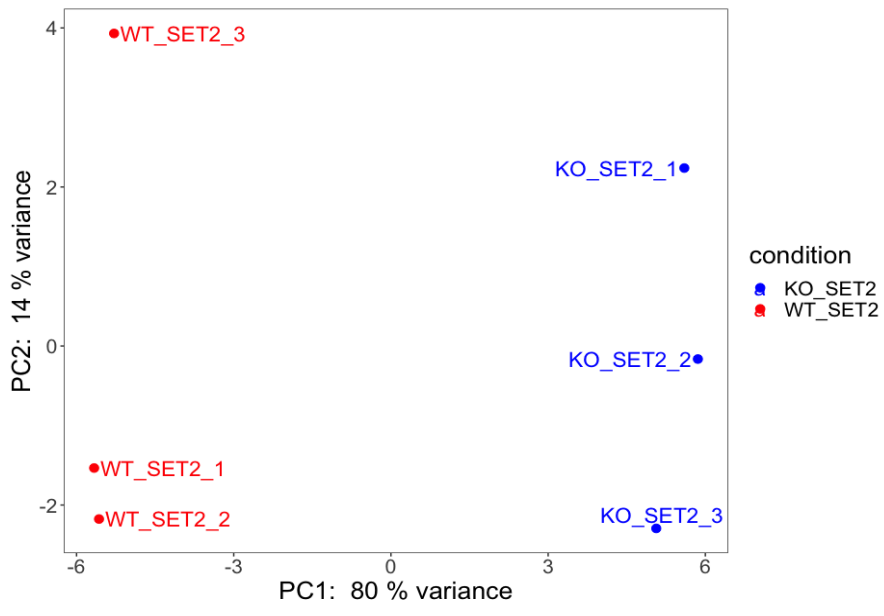

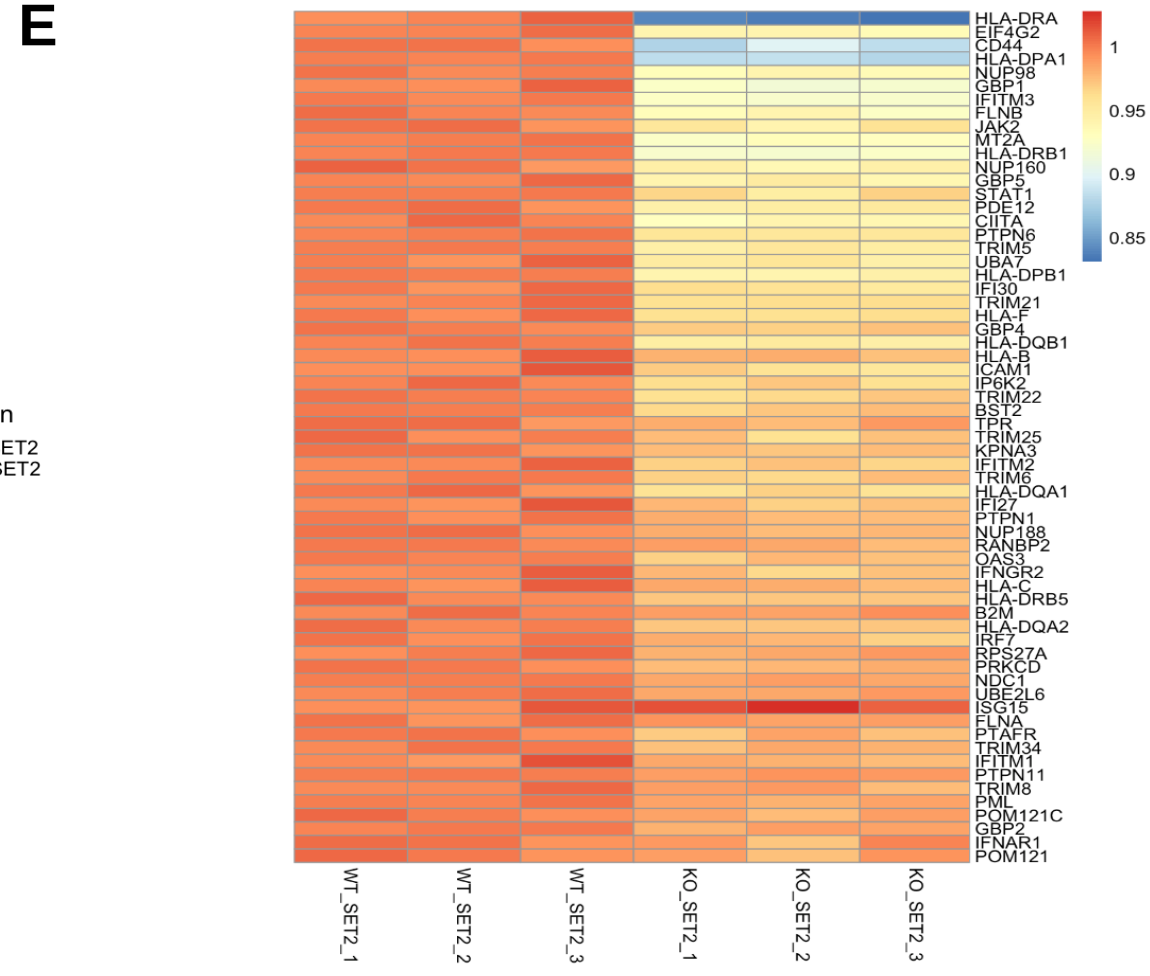

Supplementary Figure 5

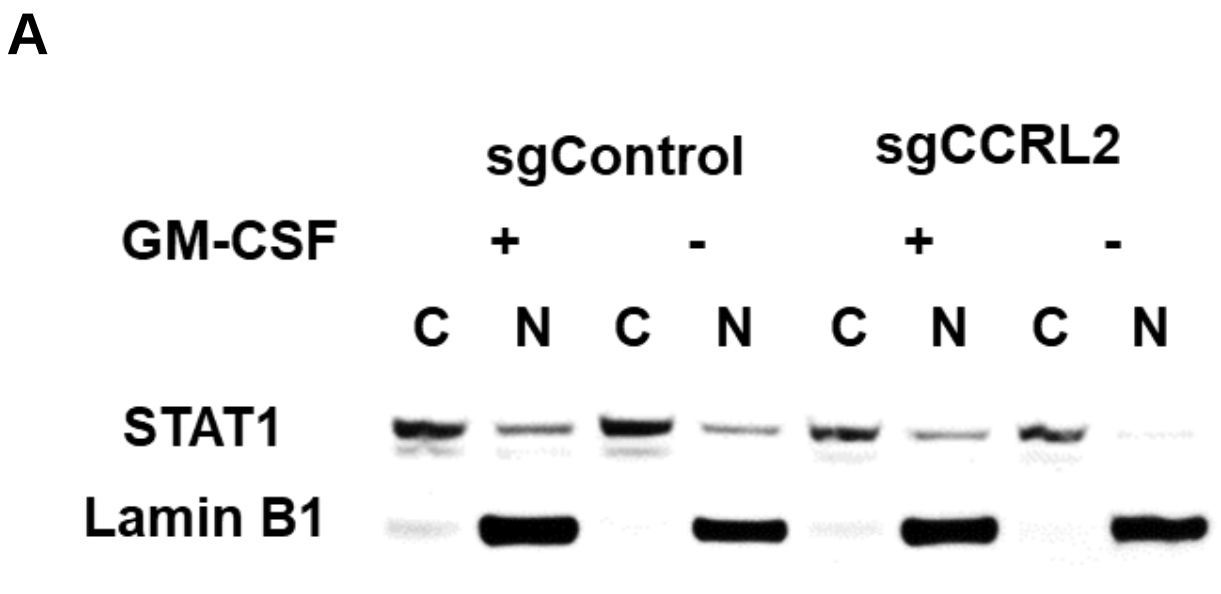

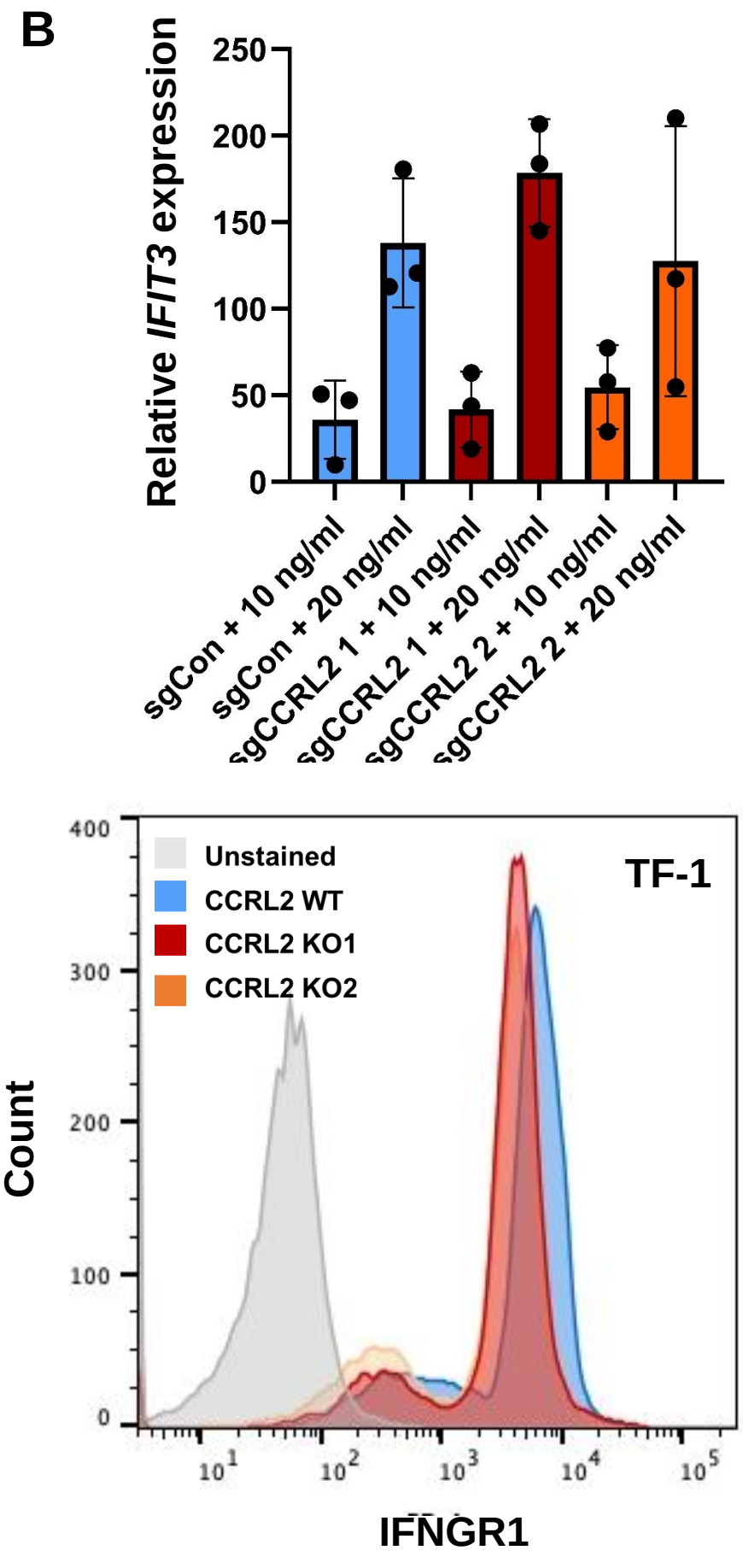

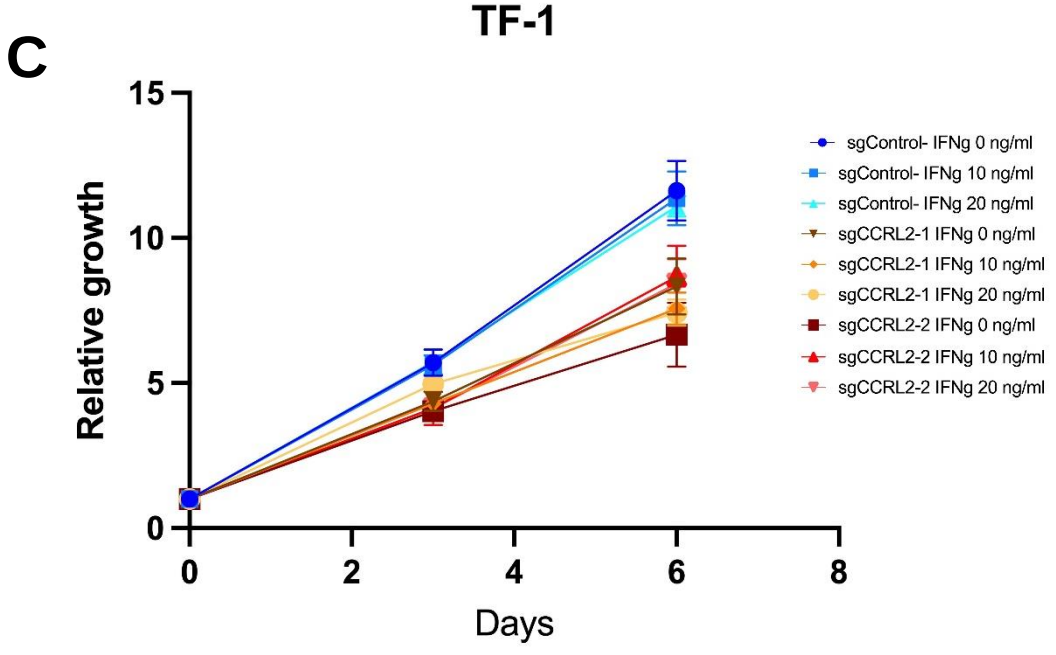

Supplementary Figure 6

A

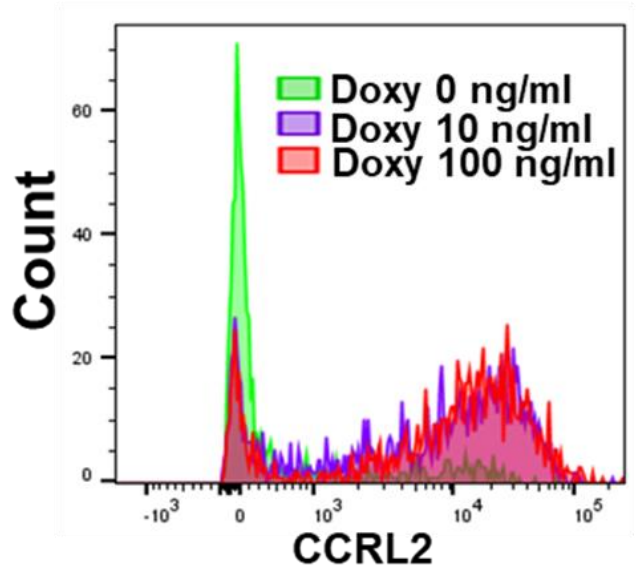

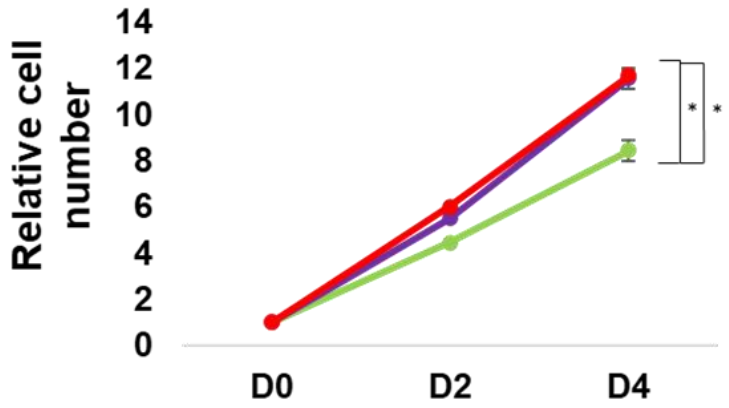

B

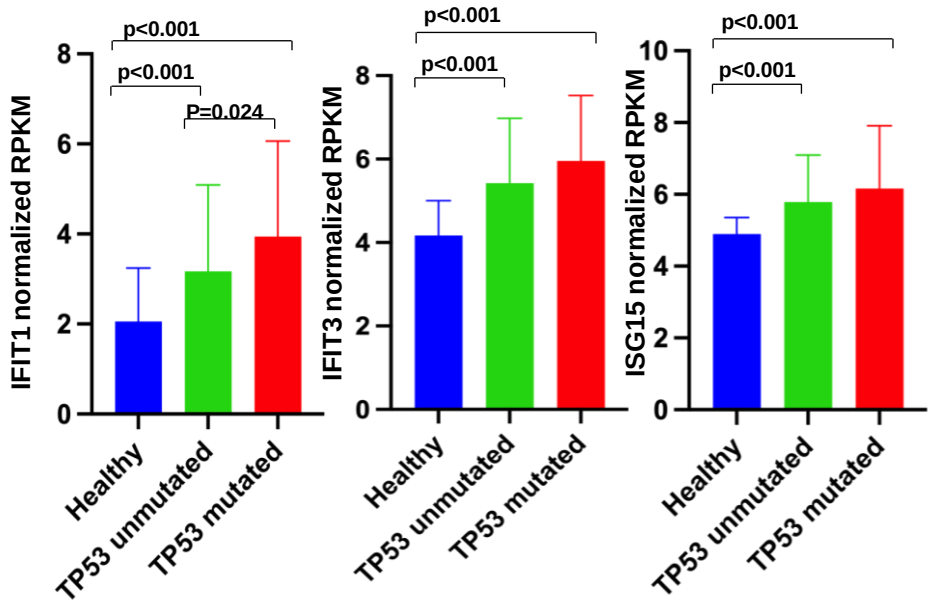

C

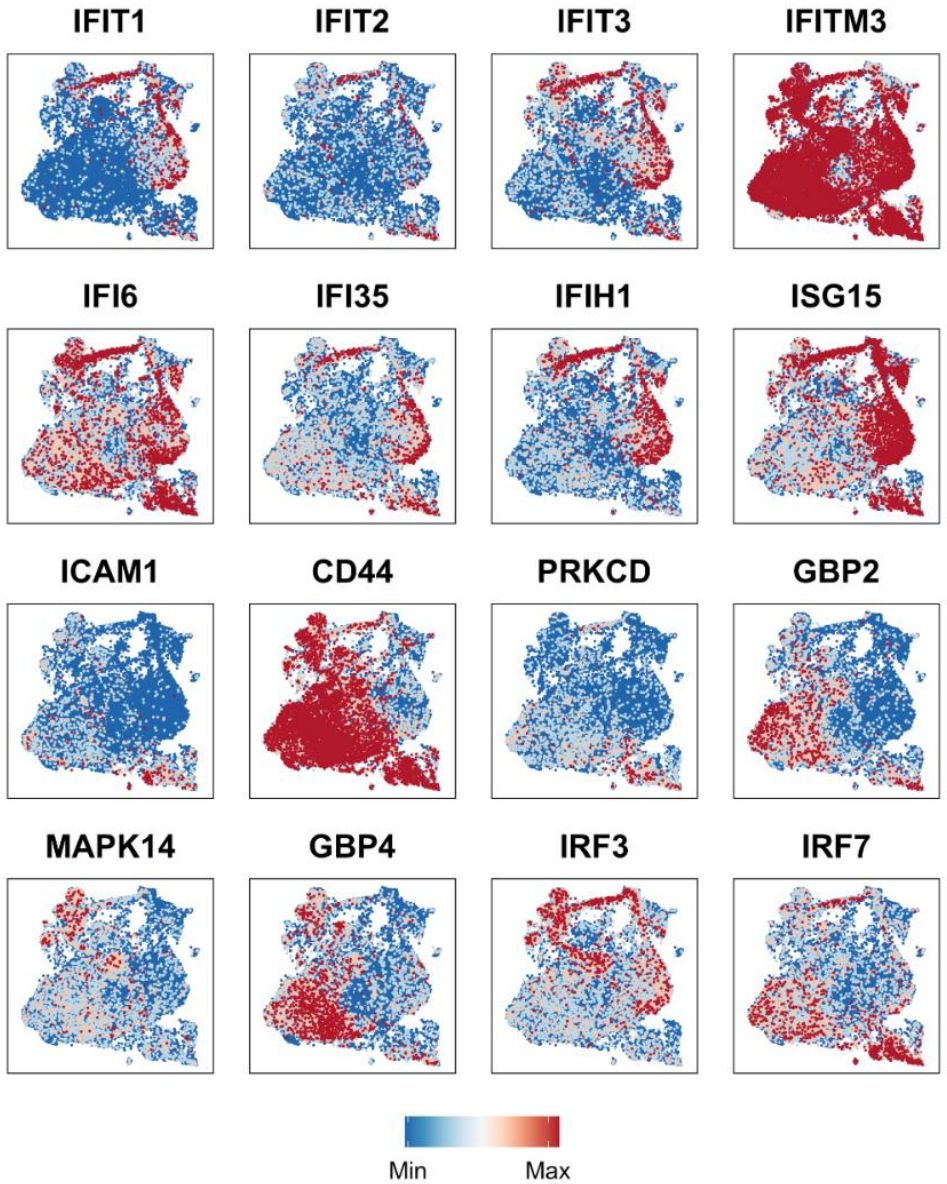

Supplementary Figure 7

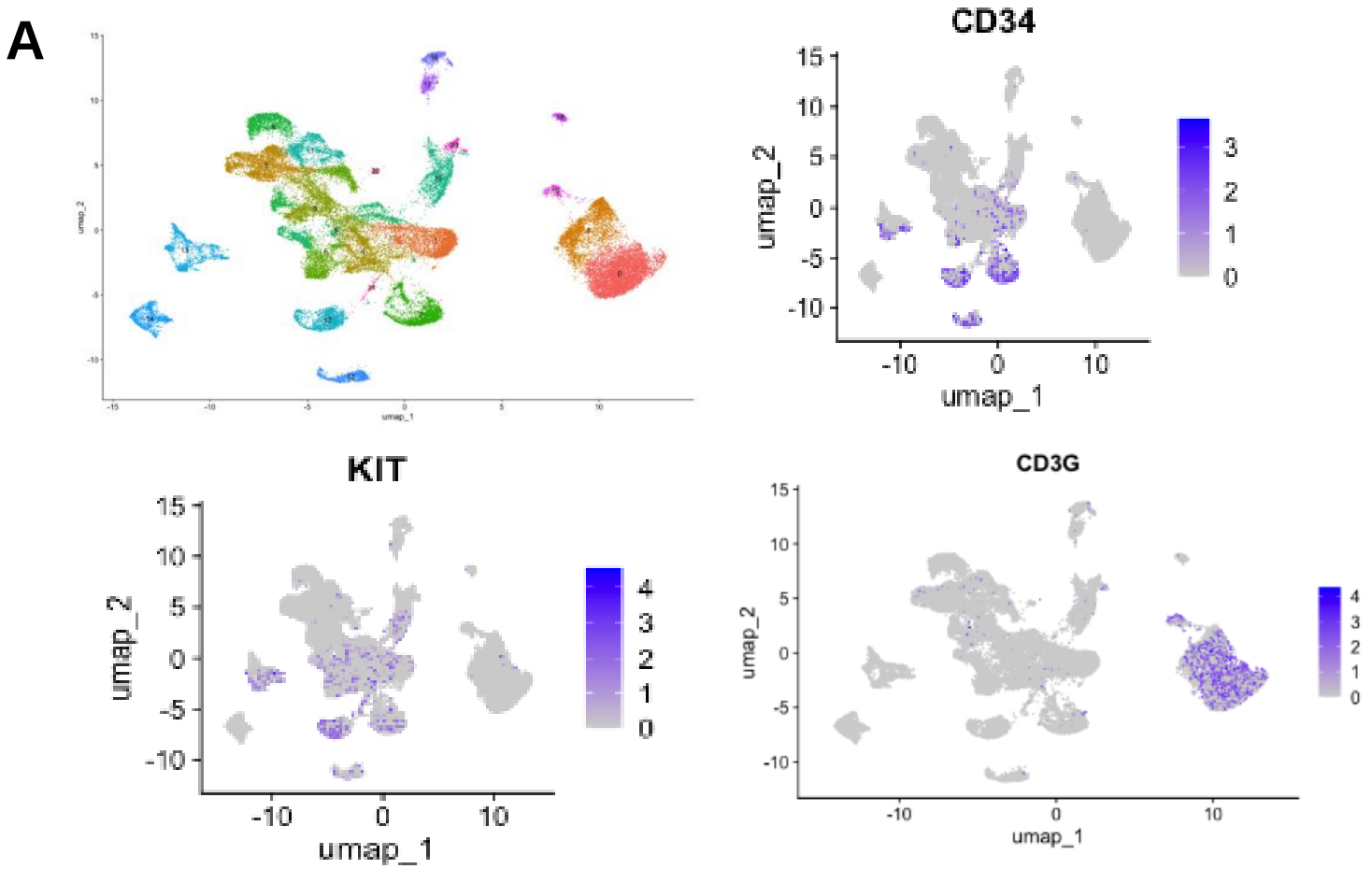

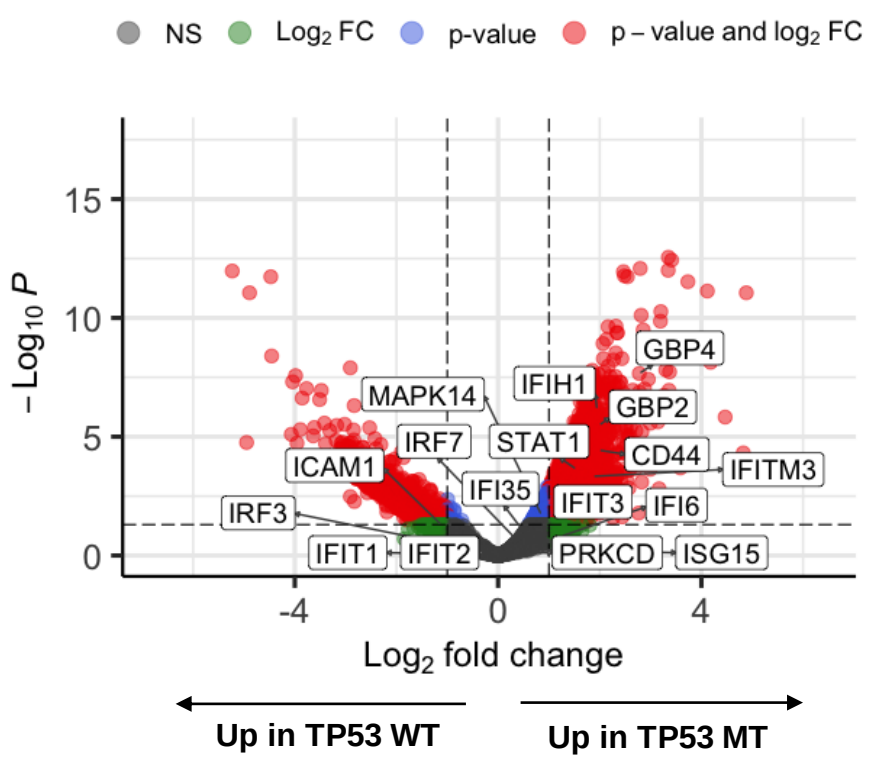

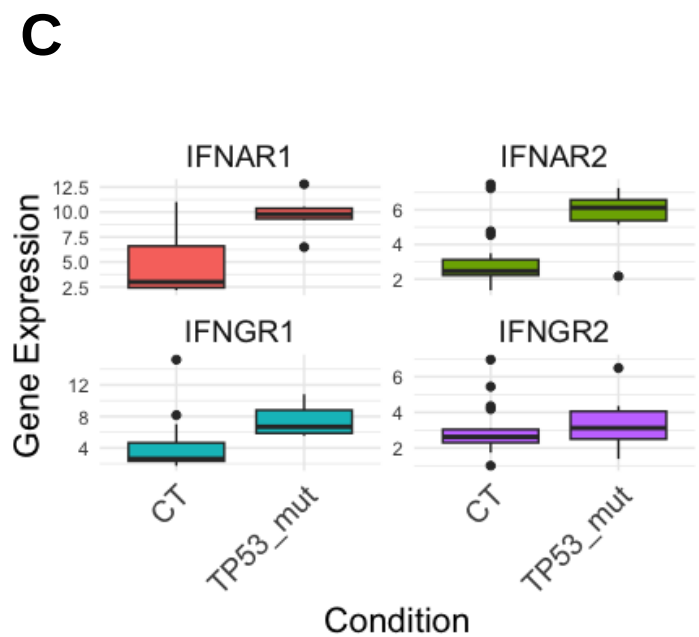

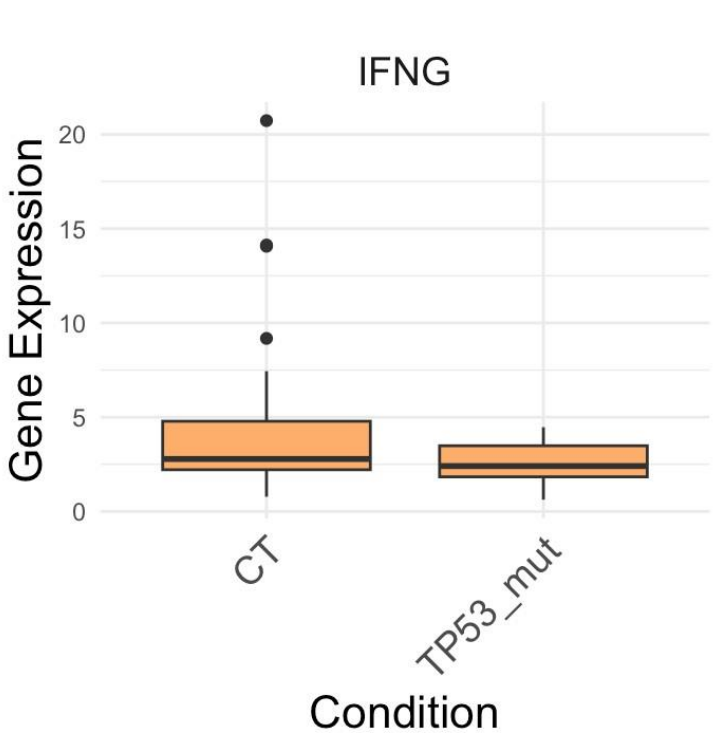

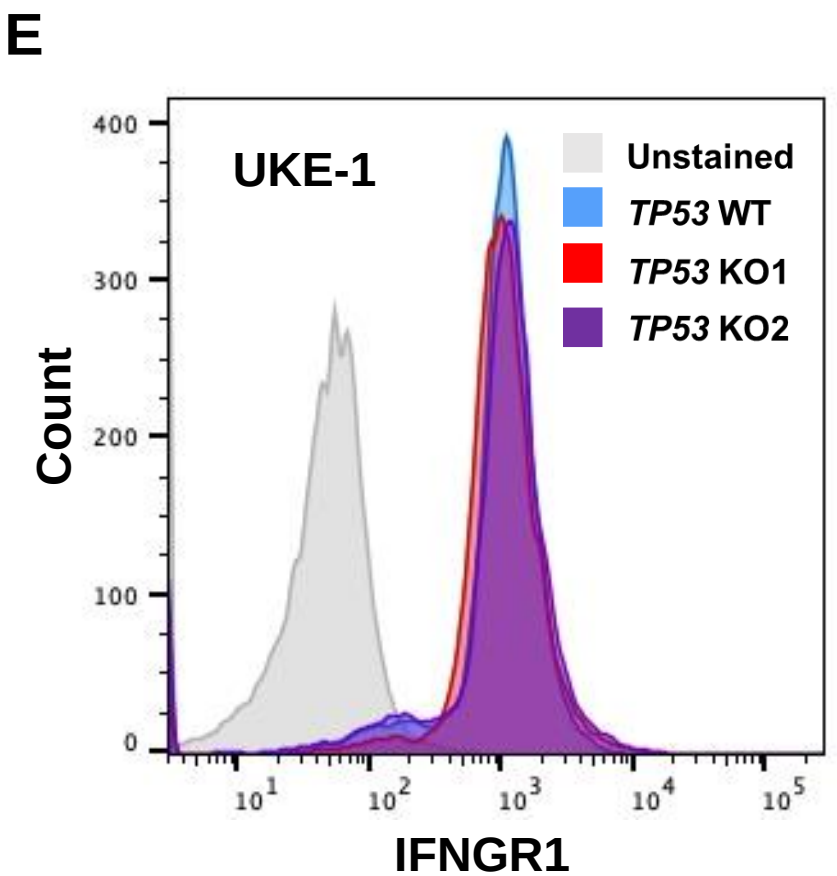

Supplementary Figure 8

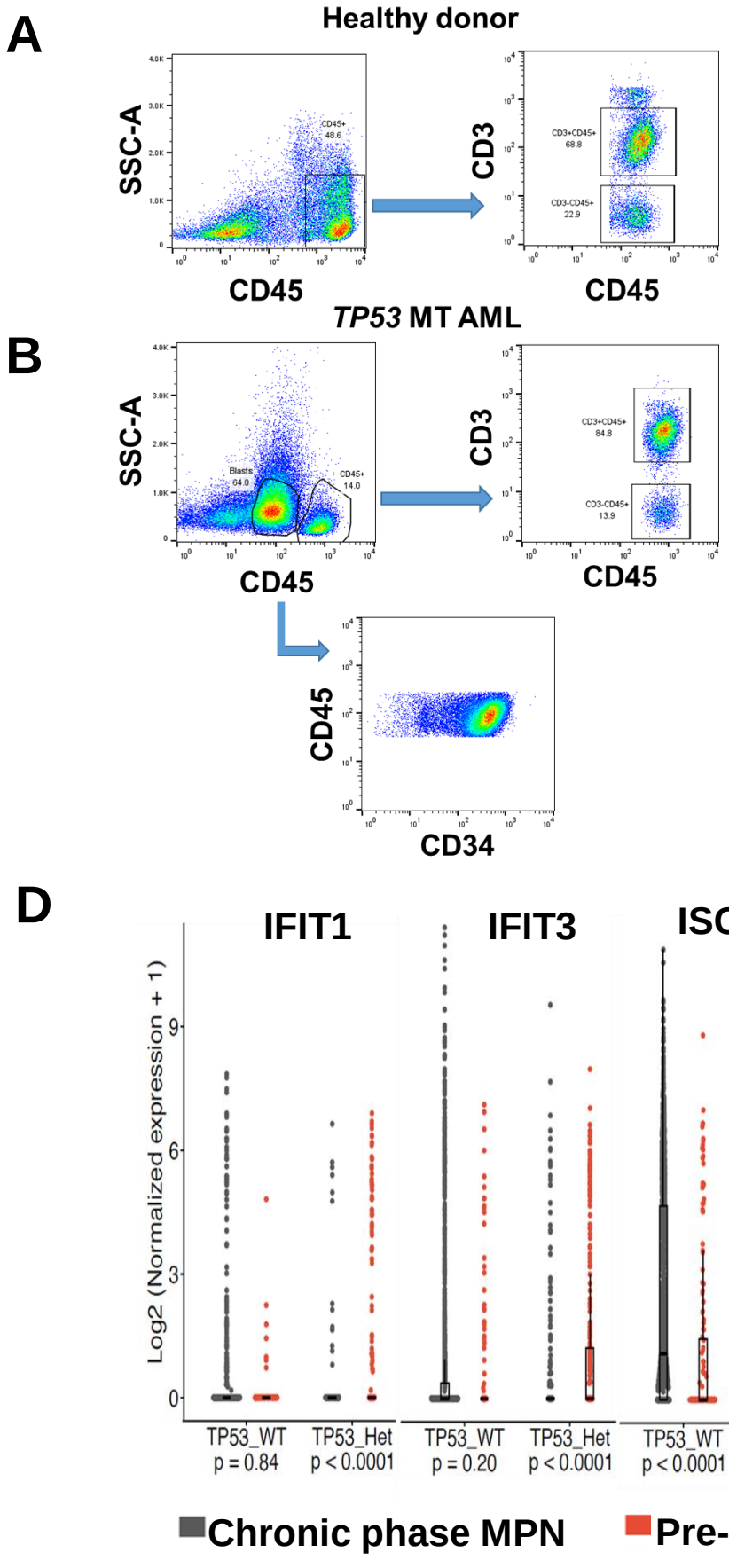

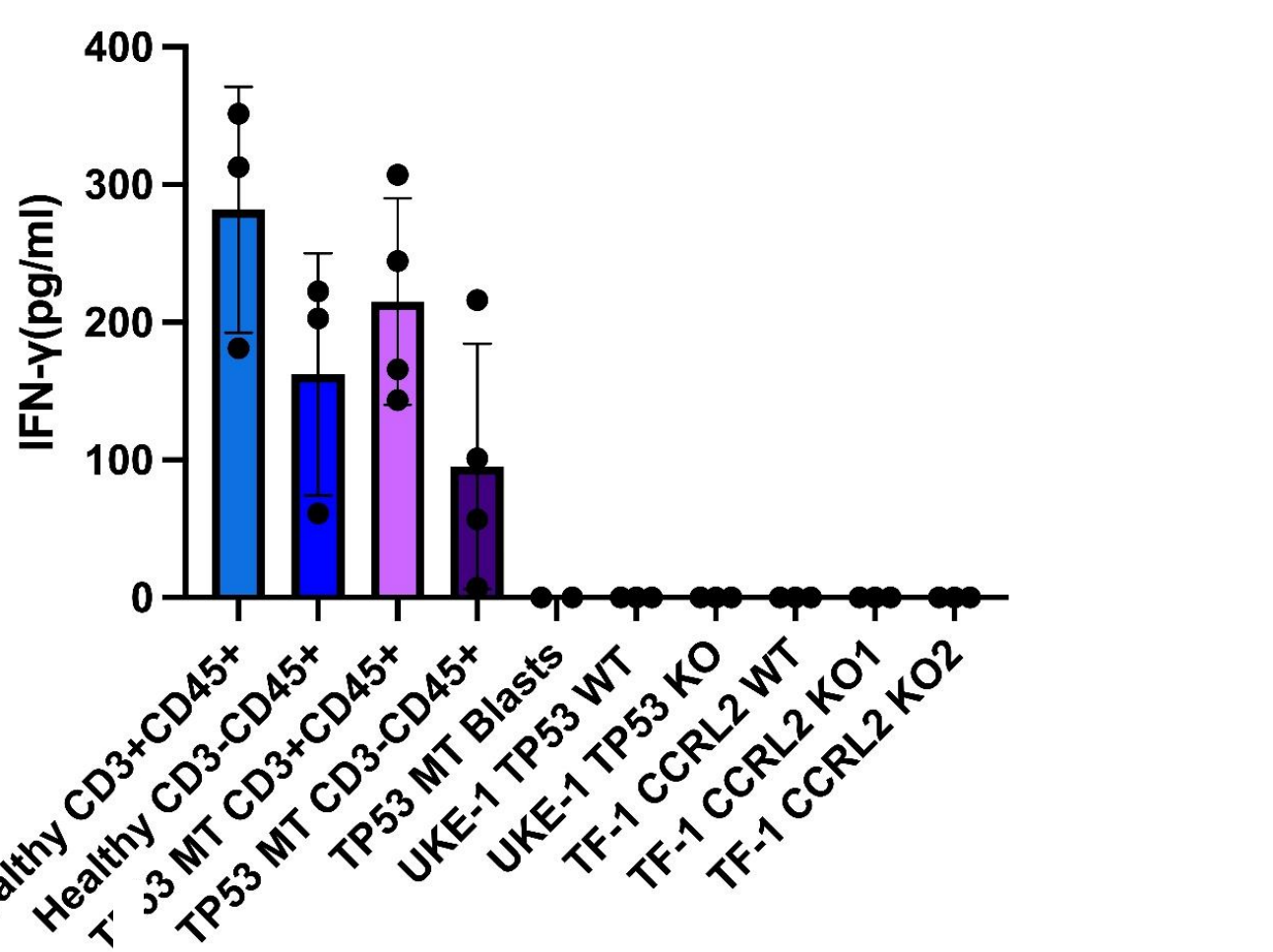

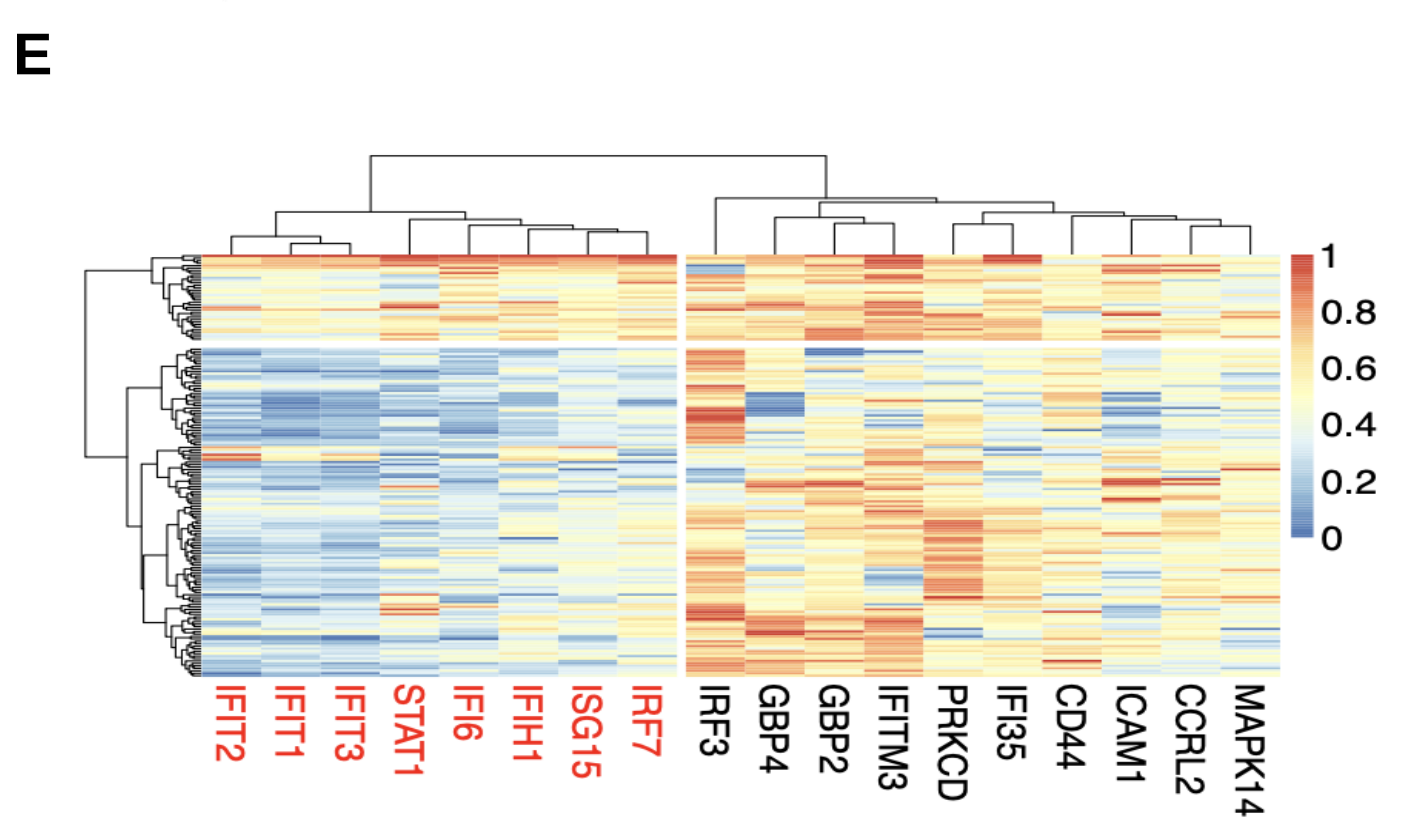

Supplementary Figure 9

Supplementary Figure Legends

Supplementary Fig. 1. (A) Genomic landscape of 15 patients with *TP53* MT MDS/AML with complex karyotype and either one *TP53* mutation of VAF at least 50% or two or more *TP53* mutations and 4 patients with AEL, which were included in the assessment of CCRL2 expression. 4 patients with *TP53* MT MDS/AML had erythroid predominance (EP) (≥50% of nucleated bone marrow cells were erythroid progenitors) but did not meet AEL criteria. **(B)** Lollipop plot showing specific TP53 variants of the patients' samples

Supplementary Fig.2. (**A)** Gating strategy for analysis of healthy donors' samples based on CD34/CD71/CD235a expression. **(B)** Gating strategy for analysis of TP53 mutated MDS/AML and AEL samples based on SSC-A/CD45 to identify blasts which express high CD71/CCRL2 (for AEL patients) and CD34/CD71 expression to identify CD34+CD71+ cells (for AEL patients). **(C-D)** *TP53* MT MDS/AML patients with EP showed a trend toward higher CCRL2 expression in their blasts and CD34+ cells respectively compared to *TP53* MT MDS/AML without EP. **(E)** Assessment of CCRL2 expression by flow cytometry in bone marrow samples of 15 patients with *TP53* MT MDS/AML with complex karyotype and either one *TP53* mutation of VAF at least 50% or two or more *TP53* mutations and 4 patients with AEL. 4 patients with *TP53* MT MDS/AML had erythroid predominance (EP) (≥50% of nucleated bone marrow cells were erythroid progenitors) but did not meet AEL criteria.

Supplementary Fig. 3. (A) Western blot confirming the TP53 knockouts (KO1 and KO2) in UKE-1 cells. **(B)** qPCR showing higher CCRL2 expression in *TP53* KO UKE-1 cells compared to *TP53* WT UKE-1 cells. **(C-H)** CCRL2 knockout (KO) with two different lentiviruses (sgCCRL2 1 and sgCCRL2 2) compared to scramble sgRNA (sgControl) was confirmed by flow cytometry in TF-1, F36P, K562, SET2 and HEL cells respectively. **(I)** CCRL2 KO showed no effect on the clonogenicity of the *TP53* WT monocytic MV4-11 cells.

Supplementary Fig. 4. (A) On day 65, survived TF-1 mice were euthanized. Disease burden in bone marrow was measured by human CD45+%. Mice engrafted with sgCCRL2 had a significantly lower percentage of human CD45+ than those engrafted with sgControl (p=0.003). **(B)** Disease burden in bone marrow of SET2 engrafted mice was measured by human CD45+%. Mice engrafted with sgCCRL2 had a significantly lower percentage of human CD45+ than those engrafted with sgControl (p=0.004).

Supplementary Fig. 5. (A) Volcano plot of fold changes (FC) in protein expression between CCRL2 knockout (sgCCRL2) and wild type (sgControl) cells show the IFN-γ signaling regulator STAT1 (both long and short isoforms) along with the IFN-γ targets (IFIT1, IFIT3 and ISG15) were amongst the top downregulated proteins by CCRL2 KO. LXR/RXR targets are upregulated in CCRL2 KO cells. **(B)** Protein-protein interaction network showing that CCRL2 positively regulates IFN-γ signaling and suppresses LXR/RXR activation. **(C)** Bulk RNA-seq was performed followed by gene set enrichment analysis (GSEA) using a compilation of pathways from MSigDB in CCRL2 WT or KO SET2 cells. Volcano plot portrays the expression of the differentially expressed genes. **(D)** Principal components analysis showing principal components 1 and 2 (PC1 and PC2) variances for SET2 WT and KO cells. **(E)** Heatmap shows that IFN-γ gene networks was found to be the top CCRL2-regulated pathway.

Supplementary Fig. 6. (A) CCRL2 KO decreased the nuclear translocation of STAT1 in TF-1 cells (C: cytoplasm, N: nucleus). **(B)** Treatment of TF-1 CCRL2 KO and WT cells with 10 ng/ml and 20 ng/ml of IFN-γ showed that CCRL2 KO had no effect on the upregulation of *IFIT3* expression as a response to exogenous IFN-γ. **(C)** Treatment of TF-1 CCRL2 WT and KO cells with two doses of IFN-γ (10 ng/ml and 20 ng/ml) showed no impact on cells growth in the presence

or absence of CCRL2 expression. **(D)** CCRL2 KO caused a modest suppression of IFN-γ receptor (IFNGR) levels in the surface of TF-1 cells in the absence of exogenous IFN-γ.

Supplementary Fig. 7. (A) Doxycycline (doxy)-inducible CCRL2 TF-1 cell model upon treatment with 10 or 100 ng/ml doxycycline induced CCRL2 expression and increased their growth at 2 and 4 days ($p=0.008$ for 10 ng/ml and $p=0.003$ for 100ng/ml). **(B)** Comparison of the expression of *IFIT1*, *ISG15* and *IFIT3* between *TP53* WT and *TP53* MT AML samples was done by analyzing RNA sequencing data derived from Beat AML dataset. *IFIT1* was found to be significantly overexpressed in *TP53* MT AML samples compared to *TP53* WT ones ($p=0.024$). All three CCRL2/STAT1 target genes were upregulated in AML samples compared to healthy bone marrow mononuclear cells ($p<0.001$). **(C)** Analysis of single-cell RNA sequencing data from Kuusanmäki et al. showed that blasts with erythroid differentiation express higher levels of various CCRL2/IFN-γ targets including *IFIT1*, *IFIT2*, *IFIT3*, *IFI35*, *IFIH1* and *ISG15* compared to other AML differentiation clusters.

Supplementary Fig. 8. (A) Analysis of single cell RNA sequencing data from van Galen et al. identified blasts from bone marrow aspirates of 16 AML patients including 3 individuals with *TP53* mutations by CD34 and c-KIT (CD117) expression and T-cells by CD3 expression. **(B)** Volcano plot showing that most of the CCRL2/IFN-γ associated genes are overexpressed in *TP53* MT AML cells compared to *TP53* WT ones. **(C)** *IFNGR1* and *IFNGR2* show a very modest upregulation in *TP53*-mutated AML samples (p-adjusted= 0.051 and 0.860 respectively) compared to blasts from *TP53* WT AML patients, as shown in the Gene expression BoxPlot. Each dot in the boxplot represents the pseudobulk aggregated expression data for one study participant normalized by a size factor as implemented in DESeq2. (**D**) Comparison of *IFNG* in T-cells of *TP53* WT and MT AML patients based on single cell RNA sequencing data from van Galen et al.

showing that patients with *TP53* MT AML did not express higher levels of *IFNG* compared to the WT ones. (**E**) *TP53* deletion in UKE-1 cells did not affect the expression of IFNGR1 in cells surface.

Supplementary Fig.9 (A) Sorting of CD3+CD45+ and CD3-CD45+ cells from 4 *TP53* mutated AML patients and 3 healthy bone marrow donors. **(B)** Blasts by dim CD45 and low side scatter were also sorted from the *TP53* mutated AML patients. **(C)** Cells (50,000 cells/ml) were cultured for 72 hours and levels of IFN-γ were then measured by ELISA, showing that T-cells from *TP53* MT AML cells secreted relatively lower IFN-γ levels compared to healthy donors. Blasts from TP53 mutated AML patients, UKE-1 TP53 WT and KO and TF-1 CCRL2 WT and KO cells were not found to secrete any IFN-γ. **(D)** Analysis of publicly available single-cell RNA sequencing data showed that pre-leukemic *TP53* heterozygous clones from patients with myeloproliferative neoplasms (MPN) who transformed to multi-hit *TP53* mutated sAML have higher expression of *IFIT1* ($p<0.0001$), *IFIT3 (*$p<0.0001$) and *ISG15* ($p<0.0001$) compared to *TP53* heterozygous clones from patients who remained in chronic phase (CP-MPN). **(E)** Heatmap showing the unsupervised clustering of genes and patients, considering the scaled gene expression values. Both rows and columns of the heatmap were cut in two based on dendrogram height. Through this, we separated the patients in two clusters based on the expression pattern of the CCRL2/IFN-γ targets: Cluster 2 patients ($n = 35$) who presented a high expression of *IFIT2, IFIT1, IFIT3, STAT1, IFI6, IFIH1, ISG15, IRF7*, whereas Cluster 1 patients ($n = 134$) contained the rest of the patients.

Supplementary Methods

Patients and sample processing

Normal marrow was collected as excess material after harvesting normal donors for allogenic bone marrow transplantation. All specimens were obtained by the Johns Hopkins Kimmel Cancer Center Specimen Accessioning Core. Isolation of CD34+ cell subsets was performed using the CD34 MicroBead kit (Miltenyi Biotec) as before[12, 13].

Cell lines and reagents

TF-1 cells and F36P cells were cultured in RPMI 1640 (Thermo Fischer Scientific, Waltham, MA) with 10% and 20% fetal bovine serum (FBS) (MilliporeSigma, Burlington, MA) respectively with the addition of GM-CSF (2 ng/ml and 20 ng/ml respectively; PeproTech). K562 and UKE-1 cells were cultured in RPMI 1640 with 10% FBS. SET2 and HEL cells were cultured in RPMI 1640 with 10% FBS. MV4-11 cells were cultured in IMDM (Thermo Fischer Scientific, Waltham, MA) with 10% FBS. All the cell lines were cultured with 2mM L-glutamine, penicillin (100 U/ml) and streptomycin (100µg/ml) at 37 in 5% CO2. Doxycycline was purchased from Sigma Aldrich (D9891) and was diluted in PBS (Thermo Fischer Scientific, Waltham, MA).

Flow cytometry analysis

Gating was based on an unstained control. Following staining, analysis was performed using BD LSR II (BD Biosciences). Mean fluorescence intensity (MFI) was measured for each marker using FlowJo analysis software version 10.0.8(FlowJo, Ashland, CO, USA).

CCRL2 and TP53 knockout

TF-1, F36P, K562, SET2, HEL and MV-411 cells were incubated with the viral supernatant and polybrene (8µg/ml; MilliporeSigma) for transduction. 48 hours later, cells were treated with

puromycin (2µg/ml for TF-1 and K562, 1.5 µg/ml for F36P, 0.5 µg/ml for SET2 and HEL and 0.75 µg/ml for MV4-11) for 3-4 days for resistant cells selection.

Similarly, lentiviral vectors expressing TP53-targeting sgRNA (or empty were transfected into 293T cells as detailed above. UKE-1 cells were incubated with the viral supernatant and polybrene (8µg/ml; MilliporeSigma) for transduction. 48 hours later, cells were treated with Blasticidin (10 µg/ml) for 3-4 days for resistant cells selection.

Colony formation assay

Clonogenic assays were conducted as previously detailed [12, 13]. Cells were counted and resuspended at a density of 3000 cells/ml in methylcellulose-based media. Following around two weeks of incubation at 37°C in 5% CO2, counting of colony forming units was performed under bright-field microscopy.

TF-1 and SET2 xenograft mice

After transduction of TF-1 and SET2 cells with sgRNAs, and selection of resistant cells as above, resistant cells were transduced with a GFP/Luciferase+ retroviral vector as before [12, 13]. Afterward, GFP+ cells sorted, and injected intravenously to 8-10-week-old NOD.Cg-*Prkdc*^{scid} *Il2rg*^{tm1Wjl}/SzJ (NSG) female mice (10^6 cells per mouse). Using IVIS spectrum in vivo imaging system, bioluminescence signal was measured. At day 65 for TF-1 and 60 for SET2, all remaining mice were euthanized, and the percentage of human CD45+ cells was assessed in bone marrow by flow cytometry. Our study has been performed under a mouse protocol approved by the Johns Hopkins University Animal Care and Use Committee (IACUC).

Mass spectrometry phosphoproteomics analysis

Protein extracts were buffer exchanged using SP3 paramagnetic beads (GE Healthcare)[43]. Briefly, protein samples (20 ug) were brought up to 100 uL with 10 mM TEAB + 1% SDS and disulfide bonds reduced with 10 uL of 50 mM dithiothreitol for 1 hour at 60C. Samples were cooled to RT and pH adjusted to ~7.5, followed by alkylation with 10 uL of 100 mM iodoacetamide in the dark at RT for 15 minutes. Next, 100 ug (2 uL of 50 ug/uL) SP3 beads were added to the samples, followed by 120 uL 100% ethanol. Samples were incubated at RT with shaking for 5 minutes. Following protein binding, beads were washed with 180 uL 80% ethanol three times. Proteins were digested on-bead with 2ng trypsin (Pierce) in 100uL 25mM TEAB buffer at 37C overnight. Resulting peptides were separated from the beads using a magnetic tube holder. Supernatants containing peptides were acidify and desalted on u-HLB Oasis plates. Peptides were eluted with 60% acetonitrile/0.1%TFA and dried using vacuum centrifugation.

Each of the 12 dried peptide samples were labeled with one of the unique TMTpro 16-plex reagents (Thermo Fisher, Lot WK338750) according to the manufacturer's instructions. All 12 TMT labeled peptide samples were combined and dried by vacuum centrifugation.

The combined TMT-labeled peptides were re-constituted in 100 µL 200mM TEAB buffer and filtered through Pierce Detergent removal columns (Fisher Scientific PN 87777) to remove excess TMT label. Peptides in the flow through were diluted to 2 mL in 10 mM TEAB in water and loaded on a XBridge C18 Guard Column (5 µm, 2.1 x 10 mm, Waters) at 250 µL/min for 8 min prior to fractionation on a XBridge C18 Column (5 µm, 2.1 x 100 mm column (Waters) using a 0 to 90% acetonitrile in 10 mM TEAB gradient over 85 min at 250 µL/min on an Agilent 1200 series capillary HPLC with a micro-fraction collector. Eighty-four 250 ul fractions were collected and concatenated into 24 fractions[44]. From each fraction, 10% was analysis for global quantitative

proteomic comparison and normalization. The remaining 90% was combined into 12 fractions for phosphopeptide enrichment by binding to titanium dioxide (TiO2)[45].

TMT labeled peptides before and after phosphopeptide enrichment were analyzed by nanoflow reverse phase chromatography coupled with tandem mass spectrometry (nLCMS/MS) on an Orbitrap-Fusion Lumos mass spectrometer (Thermo Fisher Scientific) interfaced with an EasyLC1000 UPLC. Peptides will be separated on a 15 cm × 75 μm i.d. self-packed fused silica columns with ProntoSIL-120-5-C18 H column 3 μm, 120 Å (BISCHOFF) using an 2-90% acetonitrile gradient over 85 minutes in 0.1% formic acid at 300 nl per min and electrosprayed through a 1 μm emitter tip (New Objective) at 2500 V. Survey scans (MS) of precursor ions were acquired with a 2 second cycle time from 375-1500 m/z at 120,000 resolution at 200 m/z with automatic gain control (AGC) at 4e5 and a 50 ms maximum injection time. Top 15 precursor ions were individually isolated within 0.7 m/z by data dependent monitoring and 15s dynamic exclusion and fragmented using an HCD activation collision energy 39. Fragmentation spectra (MS/MS) were acquired using a 1e5 AGC and 118 ms maximum injection time (IT) at 50,000 resolution.

Fragmentation spectra were processed by Proteome Discoverer (v2.4, ThermoFisher Scientific) and searched with Mascot v.2.8.0 (Matrix Science, London, UK) against RefSeq2021_204 database. Search criteria included trypsin enzyme, two missed cleavage, 5 ppm precursor mass tolerance, 0.01 Da fragment mass tolerance, with TMTpro on N-terminus and carbamidomethylation on C as fixed modifications and TMTpro on K, phosphorylation on S, T or Y, oxidation on M, deamidation on N or Q as variable modifications. Peptide identifications from the Mascot searches were processed within PD2.4 using Percolator at a 5% False Discovery Rate confidence threshold, based on an auto-concatenated decoy database search. Peptide spectral matches (PSMs) were filtered for Isolation Interference <25%. Relative protein abundances of

identified proteins were determined in PD2.4 from the normalized median ratio of TMT reporter ions from the top 30 most abundant proteins identified. Technical variation in ratios from our mass spectrometry analysis is less than 10% [46].

Pathway Enrichment Analysis

The raw grouped values were then transformed to log2 notation and the wild-type and knock-down values were then quantile normalized to reduce experimental noise across the three biological replicates each. A t-test analysis was then run to compare the two, WT and KO, biological classes by relative abundance, expressed as fold change, and statistical significance, expressed as p-value. Proteins that demonstrated >2SD absolute value fold change were judged to be differentially abundant, and all these results were exported to the Ingenuity Pathway Analysis (QIAGEN Inc.) platform for functional analysis.

Ingenuity Pathway Analysis, IPA, evaluated its known pathways to determines those that are enriched for proteins that demonstrated this >2SD fold change, by comparing each pathway's number of proteins that do or do-not not show this fold change. For each specific pathway IPA returned a Fisher's exact test of whether an enrichment exists, and a Z-score whether the pathway is likely inhibited or activated.

Western Blotting

Protein extraction was performed using M-PER™ Mammalian Protein Extraction Reagent (#78501). Antibodies against P-STAT1 (Tyr^{701}) (#9167), P-STAT1 (Ser^{727}) (#9177), STAT1(#9172), and ßactin (#4970) were all purchased from Cell Signaling Technology.

Co-immunoprecipitation

Cell lysates from TF-1, F36P, SET2 cells and doxy-inducible CCRL2 TF-1 cells were incubated overnight with Sepharose bead conjugate JAK2 monoclonal antibody (Cell Signaling Technology,

#4089) or Sepharose bead conjugate isotype control (Cell Signaling Technology, #3423) as previously described[12]. Beads were then washed extensively and boiled with 30 µl of loading buffer.

Single cell RNA sequencing analysis

Publicly available single cell RNA sequencing data from Kuusanmaki et al. was preprocessed as previously described [27]. Gene expression was visualized using Seurat (v5.1.0) and scCustomize (v2.0.1) in R (v4.3.1). The heatmap pertaining to this analysis was generated using ComplexHeatmap(v2.16.0).

Another publicly available single cell RNA sequencing data from van Galen et al. [28]. Gene expression was visualized using Seurat (v5.1.0) (PMID 29608179) and in R (v4.3.1). Briefly, the single cell data across samples were merged. The UMI matrix was then normalized for library size, log transformed and scaled. Principal Component Analysis (PCA) was performed followed by Louvain nearest neighbor clustering using 30 PCs. UMAP was applied to visualize the cell distribution in 2D space. A resolution of 0.5 was used for clustering to identify different cell populations. Cluster identity was identified using canonical marker genes. Differential expression (DE) analysis in individual clusters across groups of samples was performed using a pseudobulk approach. Specifically, counts across cells for each sample were aggregated using the AggregateExpression function. Surrogate variable analysis (SVA) was applied to identify latent confounders (PMID 22257669) and differential expression was estimated using DESeq2 v1.44.0 (PMID 25516281) with surrogate variables as covariates. FDR < 0.05 was set as the significance threshold.

Bulk RNA sequencing

We followed the DESeq2 pipeline (PMID 25516281) to normalize the gene expression results using a size factor that accounts for library size and gene size. This was followed by a variance stabilizing transformation as implemented in DESeq2, the output of which was used to perform principal components analysis (PCA). Surrogate variable analysis (SVA) was employed to control for unknown confounders and batch effects (PMID 22257669) while preserving the biological differences between groups. Differential expression (DE) was tested based on a Wald test with a two-tailed alternative hypothesis and a corresponding p-value was generated and adjusted for multiple testing using false discovery rate (FDR). Genes were considered significant if their FDR was < 0.05. The gene set enrichment analysis (GSEA) package was used to identify pathways enriched in our DE results (PMID 16199517).

Quantitative real-time PCR

Quantitative real-time polymerase chain reaction (PCR) was performed as previously described[47]. Total RNA was extracted using the Monarch Total RNA miniprep kit(T2010S) and complementary DNA was synthesized using QuantiTect Rev. Transcription Kit (#205311, Qiagen, Valencia, CA). Quantitative real-time PCR was conducted by using sequence-specific primers. The Radiant SYBR Green Lo-ROX qPCR kit (Alkali Scientific, Fort Lauderdale, FL) and CFX96 real-time PCR detection system (Bio-Rad) were utilized. Normalization of RNA expression was based on GAPDH expression.

Nuclear and cytoplasmic Fractionation

Nuclear/cytoplasmic fractionation was performed using the NE-PER^{TM} Nuclear and Cytoplasmic Extraction Kit (ThermoFischer Scientific #78833) as previously described[48].

Publicly available databases

Analysis of the mRNA levels of *CCRL2* and STAT1 target genes (*IFIT1, ISG15 and IFIT3*) in different subtypes of AML was based on RNA sequencing data derived from The Cancer Genome ATLAS (TCGA). Clinical and transcriptomic data in the form of RSEM values from the TCGA LAML cohort were downloaded via cBioPortal[49-51]. Only samples that had transcriptomic and FAB information available were included. Patients were grouped based on their FAB status in M6/7 and M1/2/3/4/5, the latter being labelled as "Other". A total of 171 patients from the TCGA were included. Of those, 5 (2.9%) had an FAB of M6/7. Normality of the distribution of the RSEM values was assessed using skewness and kurtosis assessment and histogram visualization. Differences between two non-normally distributed groups were evaluated using the Mann-Whitney-Wilcoxon rank sum test. A p-value under 0.05 was considered statistically significant. We calculated an overall CCRL2/IFN signaling score based on TCGA dataset using an 18 gene list: RSEM values for CCRL2, STAT1, IFIT1, ICAM1, CD44, IFIT2, PRKCD, IFIT3, IFI35, ISG15, GBP2, IFIH1, MAPK14, GBP4, IFI6, IRF3, IRF7, IFITM3 were min max scaled at the gene level. To obtain a score for every patient, we took the median of these scaled values at the patient level. Similarly, data was extracted from DepMap Portal (DepMap22Q2). TPM values for CCRL2, STAT1, IFIT1, ICAM1, CD44, IFIT2, PRKCD, IFIT3, IFI35, ISG15, GBP2, IFIH1, MAPK14, GBP4, IFI6, IRF3, IRF7, IFITM3 were min max scaled at the gene level. To obtain a score for every patient, we took the median of these scaled values at the cell line level. Using Beat AML dataset, data was extracted from http://vizome.org/aml/expression_strat/. Patients were included if DxAtSpecimenAcquisition was Acute Myeloid Leukaemia (AML) and related

precursor neoplasms or Healthy, pooled CD34+. Patients were included if Included_2018_DNAseqAnalysis was y or Healthy; pooled CD34+ and if none of the 18 included genes had n/a in the Normalized_RPKM column. A total of 407 patients were included. Of those, 12 (2.9%) were healthy CD34+, 360 (88.5%) were TP53 WT AML and 35 (8.6%) were TP53 MUT AML.Values from the RPKM_normalized column for CCRL2, STAT1, IFIT1, ICAM1, CD44, IFIT2, PRKCD, IFIT3, IFI35, ISG15, GBP2, IFIH1, MAPK14, GBP4, IFI6, IRF3, IRF7, IFITM3 were min max scaled at the gene level. To obtain a score for every patient, we took the median of these scaled values at the patient level. For overall survival using TCGA dataset, the surv_cutpoint function from the survminer package was used to determine an optimal cutoff for the CCRL2/IFN signaling score when it comes to overall survival. A patient was considered to have a high CCRL2/IFN signaling score if this score was over 0.1332826. The optimal cutoff for the RSEM values were 127.4210 for CCRL2, 161.9048 for IFIT1, 132.8000 for IFIT3, and 213.1177 for ISG15.

To determine specific expression differences (*CCRL2*, *IFIT1*, *IFIT3* and *ISG15*) between different CP-MPNs genotypes that progressed to sAML (pre-TP53-sAML) and that did not (CP-TP53-MPN), we used a previously published dataset[8]. Normalized gene expression per cell were downloaded from GSE226340 while corresponding genotyping data was downloaded from https://doi.org/10.5281/zenodo.8060602,metadata_MPNAMLp53_with_index_genotype.revised.txt.Normality of the distribution was assessed using histogram visualization and kurtosis and skewness evaluation. Differences between two non-normally distributed groups were assessed using Mann-Whitney-Wilcoxon rank sum test. Similarly, RNA expression data from DepMap Portal was analyzed to compare gene expression between different AML cell lines and data derived

from Beat AML database was used to compare the expression of CCRL2, and STAT1 targets across AML samples based on molecular profile.

For data on the effect of IFN on venetoclax resistance, we included 169 patients. If a patient presented multiple samples, we included the sample with the lower ID number. We focused on the expression of the following genes: CCRL2, STAT1, IFIT1, ICAM1, CD44, IFIT2, PRKCD, IFIT3, IFI35, ISG15, GBP2, IFIH1, MAPK14, GBP4, IFI6, IRF3, IRF7, IFITM3. The expression values were min max scaled at a gene level. The CCRL2 Signaling Score was defined at a patient level and was considered as the median scaled expression level of the included genes. Correlation between the CCRL2 Signaling Score and Venetoclax IC50 was assessed using Spearmans rho. Unsupervised clustering and its graphical representation was performed using the pheatmap package (https://github.com/raivokolde/pheatmap), using ward.D2 clustering. Mann-Whitney-Wilcoxon rank sum test was used to determine the difference in Venetoclax IC50 between Cluster 1 and 2.

Statistical Analysis

Statistical analysis was performed by using GraphPad Prism (GraphPad Software, La Jolla, CA). Mann-Whitney test was performed to assess statistical significance when comparing two groups. One-way analysis of variance (ANOVA) was performed for the comparisons of three or more groups. Dunnett's test was used for multiple comparisons. Standard deviation was used to assess centrality and dispersion.

Supplementary Table 1. Characteristics of patients with *TP53* mutated myeloid neoplasms and healthy donors

Characteristic	***TP53* mutated myeloid neoplasms (N=19)**	**Healthy donors (N=16)**
Age	65 (27 – 78)	44 (30 – 56)
Gender Females Males	 4 (21%) 15 (79%)	 6 (37.5%) 10 (62.5%)
Diagnosis *TP53* mutated MDS/AML AEL	 15 (79%) 4 (21%)	N/A
Treatment-related	6 (32%)	N/A
Blasts%	25 (5-80)	N/A
Karyotype Complex	 19 (100%)	N/A

Supplementary Table 2. Variants and variant allele frequencies of patients with *TP53* mutated myeloid neoplasms.

Variant(s)	VAF1	VAF2
R158H	79.9	
Y126H	81.9	
D281N	20.64	
H178P	82.41	
Y220C, R158H	24.5	26.7
G245S	67.5	
F270C	89.9	
Y220C	64.1	
V272M	60.5	
R175H	50.3	
c.994-1G>A	85.24	
D281N	97.54	
C275Y	52.56	
S303fs	86.5	
V272M	69.14	
R196P	50.2	
R273H, E285fs	15.98	14.4
H179R	79.3	
E286G, R273H	37.83	36.07